

1
2
3
4
5
6
7
8
9
10
11
12
13
14
15
16
17
18
19
20
21
22
23
24
25
26
27
28
29

**Sea ice break-up and freeze-up indicators for users
of the Arctic coastal environment**

John E. Walsh¹, Hajo Eicken¹, Kyle Redilla¹, Mark Johnson²

¹International Arctic Research Center, University of Alaska Fairbanks, Fairbanks AK 99775
USA

²College of Fisheries and Ocean Sciences, University of Alaska Fairbanks, Fairbanks AK
99775 USA

Correspondence to: John E. Walsh (jewalsh@alaska.edu)

July 2022

Revision for *The Cryosphere*

Abstract

30
31 The timing of sea ice retreat and advance in Arctic coastal waters varies substantially from
32 year to year. Various activities, ranging from marine transport to the use of sea ice as a
33 platform for industrial activity or winter travel, are affected by variations in the timing of
34 break-up and freeze-up, resulting in a need for indicators to document the regional and
35 temporal variations in coastal areas. The primary objective of this study is to use locally-
36 based metrics to construct indicators of break-up and freeze-up in the Arctic/Subarctic coastal
37 environment. The indicators developed here are based on daily sea ice concentrations derived
38 from satellite passive microwave measurements. The “day of year” indicators are designed to
39 optimize value for users while building on past studies characterizing break-up and freeze-up
40 dates in the open pack ice. Relative to indicators for broader adjacent seas, the coastal
41 indicators show later break-up at sites known to have extensive landfast ice. The coastal
42 indicators also show earlier freeze-up at some sites in comparison with freeze-up for broader
43 offshore regions, likely tied to earlier freezing of shallow water regions and areas affected by
44 freshwater input from nearby streams and rivers. A factor analysis performed to synthesize the
45 local indicator variations shows that the local break-up and freeze-up indicators have greater
46 spatial variability than corresponding metrics based on regional ice coverage. However, the
47 trends towards earlier break-up and later freeze-up are unmistakable over the post-1979 period
48 in the synthesized metrics of the coastal break-up/freeze-up and the corresponding regional ice
49 coverage. The findings imply that locally defined indicators can serve as key links between
50 pan-Arctic or global indicators such as sea-ice extent or volume and local uses of sea ice, with
51 the potential to inform community-scale adaptation and response.

52 *Key words:* sea ice, Arctic, break-up, freeze-up, ice concentration

53 **1. Introduction**

54 Coastal sea ice impacts residents and other users of the nearshore marine environment in
55 various ways. Perhaps most obvious is the fact that non-ice strengthened vessels require ice-
56 free waters for marine transport, which can serve purposes such as resupply of coastal
57 communities, the transport of extracted resources (oil, liquefied natural gas, mined metals),
58 migration of marine mammals (e.g., bowhead whales) and wintertime travel over the ice by
59 coastal residents. Key metrics for such uses of the nearshore marine environment are the
60 timing of break-up (or ice retreat) in the spring and the timing of freeze-up (or ice advance) in
61 the autumn or early winter.

62 Sea ice concentration thresholds have been used in various studies to determine the dates of
63 sea ice opening, retreat, advance and closing (Markus et al., 2009; Johnson and Eicken, 2016;
64 Bliss and Anderson, 2018; Peng et al., 2018; Bliss et al., 2019; Smith and Jahn, 2019). For
65 example, Bliss et al. (2019) define dates of opening and retreat as, respectively, the last days
66 on which the sea ice concentration drops below 80% and 15% before the summer minimum.
67 Corresponding metrics are used by Bliss et al. for the dates of advance and closing. An
68 emerging tendency in these and similar studies is the definition of break-up date as the date on
69 which ice concentration drops below a prescribed threshold and remains below that threshold
70 for a prescribed minimum duration (chosen to eliminate repeated crossings of the
71 concentration threshold as a result of temperature- or wind-driven changes in ice coverage
72 associated with transient weather events). A corresponding criterion is used for the freeze-up
73 date.

74 Coastal regions present special challenges in the application of such criteria. First, shorefast
75 or landfast ice (stationary sea ice held in place along the shoreline as a result of grounding

76 and/or confinement by the coast) is common in waters immediately offshore of the coast,
77 particularly in areas with shallow water. Landfast ice provides especially important sea ice
78 services because it offers a stable platform for nearshore travel, serves as a critical habitat for
79 marine mammals such as seals and polar bears (Dammann et al., 2018), and provides a buffer
80 against coastal storms (Hosekova et al., 2021). Second, sea ice concentrations derived from
81 passive microwave measurements are prone to contamination by microwave emissions from
82 land in coastal grid cells. Finally, many parts of the Arctic coastline have inlets, river deltas
83 and barrier islands that are not captured by the 25 km resolution of the passive microwave
84 product. While higher-resolution datasets permitting finer resolution of coastal sea ice are
85 available from sensors such as AMSR (Advanced Microwave Scanning Radiometer), the
86 record lengths are sufficiently shorter (about 20 years for AMSR) that trend analyses are
87 limited by a reliance on such products. Trend analysis is one of the main components of the
88 present study.

89 The primary objective of this study was to use the locally-based metrics to construct
90 indicators of break-up and freeze-up on Arctic/Subarctic coastal environments. A
91 subcomponent of this overall objective is to contribute to efforts at the national and global
92 scale to establish key sets of indicators that support sustained assessment of climate change
93 and inform planning and decision-making for adaptation action (AMAP, 2018; IPCC, 2022).
94 At the global, pan-Arctic, and U.S. national levels, indicators associated with the state of the
95 sea ice cover so far have focused on the summer minimum and winter maximum extent and
96 ice thickness (IPCC, 2022; AMAP, 2017; Box et al., 2019; USGCRP, 2017). As outlined by
97 Box et al. (2019), this approach has been motivated by the objective of describing and
98 tracking the state of key components of the global climate system. However, large-scale (pan-

99 Arctic) measures of e.g., sea-ice extent or volume are of little value and relevance to those
100 needing to adapt or respond to such change at the community or regional scale. Here, we
101 examine the timing of sea-ice freeze-up and break-up as key constraints for a range of human
102 activities and ecosystem functions in Arctic settings.

103 **2. Data and methods**

104 The primary data source is the archive of gridded daily sea ice concentrations derived from
105 the SMMR, SSM/I and SSMIS sensors onboard the Nimbus-7 and various DMSP satellites
106 dating back to November, 1978. The dataset is NSIDC-0051 of the National Snow and Ice
107 Data Center (NSIDC) and is accessible at <https://nsidc.org/data/nsidc-0051>. In the
108 construction of this dataset, the NASA Team algorithm (Cavalieri et al., 1984) and the NASA
109 Bootstrap algorithm (Comiso et al., 1986) were used to process the microwave brightness
110 temperatures into a consistent time series of daily sea ice concentrations. The data are on a
111 polar stereographic grid projection with a grid cell size of 25 km x 25 km. Prior to applying
112 these definitions, the data were processed with a linear interpolation to fill in missing daily
113 values, followed by a spatial and then temporal smoothing to filter out short (< 3 days) events.
114 Specifically, the daily sea ice concentration values were spatially smoothed using a generic
115 mean filter with a square footprint of 3 x 3 grid cells. The data were then temporally smoothed
116 three times using a Hann window.

117 The daily sea ice concentrations are used to define the metrics of the start and end of break-up
118 and freeze-up in each year of a 40-year period, 1979-2018. The definitions build on those
119 used by Johnson and Eicken (2016; hereafter denoted as J&E), which were informed by
120 Indigenous experts' observations of ice use and ice hazards in coastal Alaska, and relate to
121 planning and decision-making at the community-scale (Eicken et al., 2014). Here, we expand

122 the satellite data analysis with minor modifications of the break-up and freeze-up criteria to
123 broaden the applicability to coastal areas. Examples include imposing maximum and
124 minimum values for the thresholds computed from summary statistics of the daily sea ice
125 concentration values of relevant periods. The revised definitions are presented in Table 1 and
126 the differences relative to those of J&E are listed in Table 2.

127 While the various thresholds in Table 1 may seem somewhat arbitrary at first glance, they are
128 based on past studies and subsequent sensitivity tests. In particular, the 10% threshold is based
129 on prior work (J&E) in which sensitivities were explored. The 25%, 40% and 50% thresholds
130 in Table 1 were arrived at by testing various values and selecting values that maximized the
131 number of years with break-up and defined freeze-up dates and had the best agreement with
132 years of indigenous observations. The selected values were those that generally maximized the
133 number of such years across the various coastal locations and MASIE regions.

134

135

136

137

138

139

140

141
142
143
144
145
146
147
148
149
150
151
152
153
154
155
156
157
158
159
160
161
162

Table 1. Definition of the start and end of break-up and freeze-up.

Break-up start The date of the last day for which the previous two weeks' ice concentration always exceeds a threshold computed as the maximum of (a) the winter (January-February) average minus two standard deviations and (b) 15%. Undefined if the average summer sea ice concentration (SIC) is greater than 40% or if the subsequent break-up end is not defined.

Break-up end The first date after the break-up start date for which the ice concentration during the following two weeks is less than a threshold computed as the maximum of (a) the summer (August-September) average plus one standard deviation and (b) 50%. Undefined if the daily SIC is less than the threshold for the entire summer or if break-up start is not defined.

Freeze-up start: The date on which the ice concentration exceeds for the first time a threshold computed as the maximum of (a) the summer (August-September) average plus one standard deviation and (b) 15%. Undefined if the daily SIC never exceeds this threshold, if the mean summer SIC is greater than 25%, or if subsequent freeze-up end is not defined.

Freeze-up end: The first date after the freeze-up start date for which the following two weeks' ice concentration exceeds a threshold computed as the maximum of (a) the average winter (January-February) ice concentration minus 10% and (b) 15%, and the minimum of this result and (c) 50%. Undefined if daily SIC exceeds this threshold for every day of the search period or if freeze-up start is not defined.

163 Table 2. Changes in the indicator definitions relative to Johnson and Eicken (2016), denoted
164 as “J&E”. The symbol “ σ ” denotes standard deviation; “sic” denotes sea ice concentration.

165 *Break-up start:*

166 - minimum sic threshold created at 15% (J&E: last day exceeding Jan-Feb mean minus 2σ)

167 - undefined if average summer sic $> 40\%$ (J&E: no such criterion)

168 - undefined if subsequent breakup end date not defined (J&E: no such criterion)

169

170 *Break-up end:*

171 - first time sic below threshold for 2 weeks instead of last day below threshold

172 (J&E: last exceeding larger of Aug-Sep mean or 15%)

173 - minimum threshold 50% (J&E: minimum threshold of 15%)

174 - undefined if break-up start not defined (J&E: no such criterion)

175

176 *Freeze-up start:*

177 - first day on which sic exceeds Aug-Sep average by 1σ (J&E: same)

178 - undefined if mean summer sic $> 25\%$ (J&R: no such criterion)

179 - undefined if subsequent freeze-up end not defined (J&E: same)

180

181 *Freeze-up end:*

182 - first time sic above threshold for following 2 weeks instead of first day above threshold

183 (threshold is Jan-Feb average minus 10%, as in J&E)

184 - thresholds imposed: Minimum (15%) and maximum (50%) (J&E: no such thresholds)

185 - undefined if sic always exceeds threshold (J&E: same)

186 Our evaluation of the coastal indicators includes comparisons of the various dates (break-
187 up/freeze-up start/end) at nearshore locations with the corresponding metrics for broader areas
188 of the Arctic Ocean and the subarctic seas. A set of ten locations was selected on the basis of
189 their geographical distribution and the relevance of local sea ice to uses by communities,
190 industry, military or other stakeholders. These locations are listed in Table 3, together with
191 their geographic coordinates. While there is admittedly some subjectivity in the selection of
192 these sites, our priorities were (1) a pan-Arctic geographical distribution, thereby expanding
193 the emphasis on North American locations in past studies (see Discussion in Section 4) and
194 (2) inclusion of locations with a mix of users affected by sea ice: Indigenous communities,
195 industry, military and other stakeholders. For each of these locations, several passive
196 microwave grid cells close to (but not adjacent to) the coastline were selected for calculation
197 of the break-up and freeze-up metrics. More specifically, the contamination of the passive
198 microwave-derived ice concentrations by the presence of land in a grid cell required the
199 exclusion of grid cells containing land. Therefore, the selected grid cells satisfied the criterion
200 that they were the cells closest to the coast but centered at least 25 km from the coast. Figure
201 1 shows geographical insets illustrating the proximity of the selected grid cells to the
202 coastline.

203 With regard to the grid cell selection, we experimented with the grid cell selections at Sabetta
204 and Utqiagvik. When the grid cell locations were one shifted offshore by one pixel at Sabetta,
205 the mean break-up start and end dates changed by only -0.1 and -1.1 days, respectively; the
206 corresponding changes in the freeze-up start and end dates were 0.2 and -0.7 days,
207 respectively. At Utqiagvik, the offshore shift resulted in an earlier mean break-up start by 3.3
208 days and a later mean break-up end by 2.9 days. The earlier break-up start is consistent with

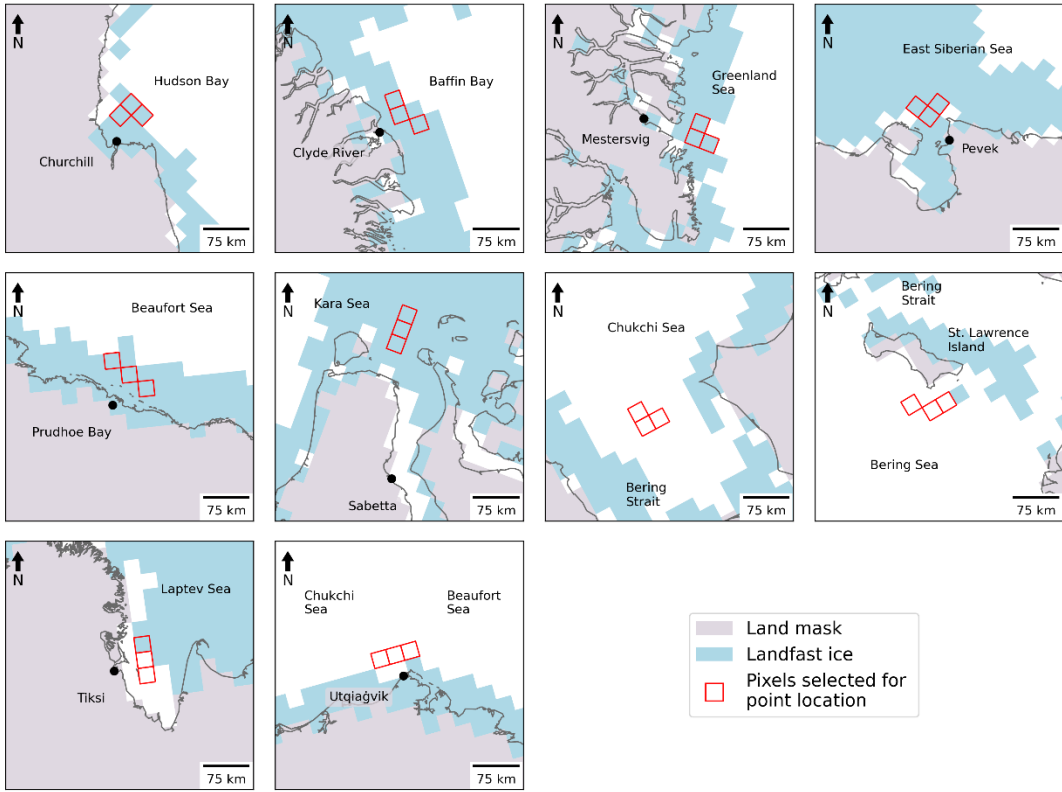
209 the presence of fast ice at the coast, as discussed in Section 4. The changes in Utqiagvik’s
 210 freeze-up dates were small when the pixels were shifted offshore, where the start of freeze-up
 211 occurred 1.1 days later and the end of freeze-up 1.1 days earlier than closer to the coast.

212

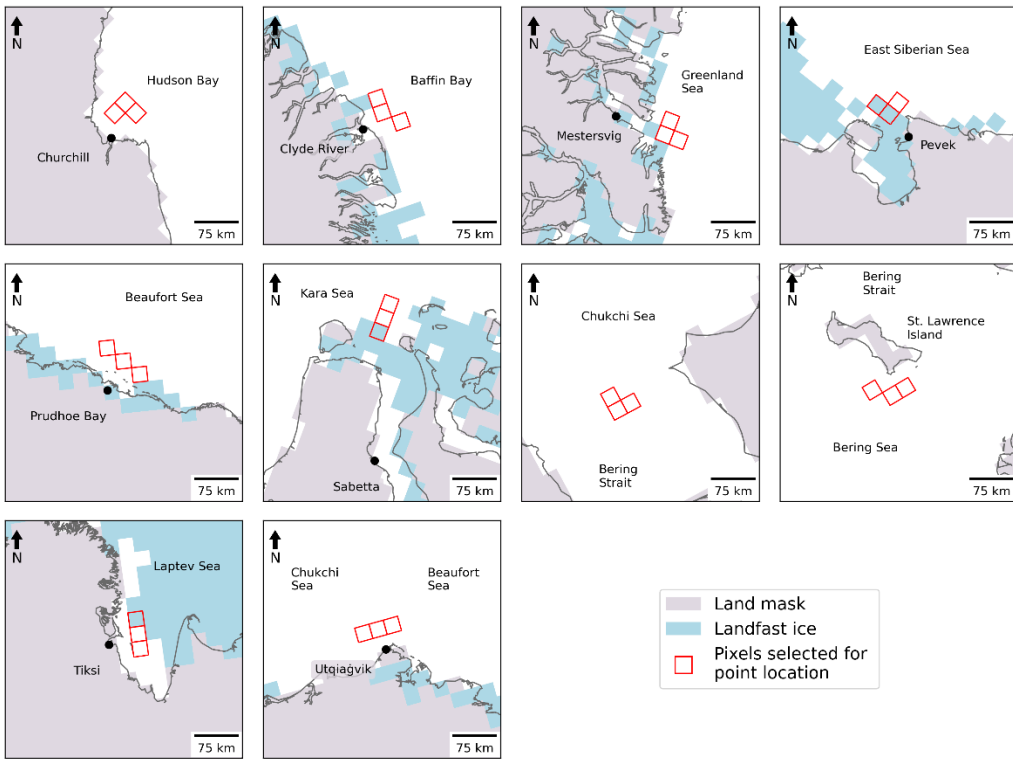
213 Table 3. Near-coastal locations selected for calculation of break-up and freeze-up metrics

214	<u>Sea</u>	<u>Location</u>	<u>Latitude, Longitude</u>	<u>Significance of location</u>
215	Beaufort Sea	Prudhoe Bay	70.2N, 148.2W	oil facilities
216	Chukchi/Beaufort Seas	Utqiagvik	71.3N, 156.8W	Indigenous community
217	Chukchi Sea	Chukchi Sea	69.6N, 170W	shipping route
218	Bering Sea	St. Lawrence Island	65.7N, 168.4W	Indigenous community
219	East Siberian Sea	Pevek	69.8N, 170.6E	port, mining facility
220	Laptev Sea	Tiksi	71.7N, 72.1E	research site, port
221	Kara Sea	Sabetta	71.3N, 72.1E	port, LNG facility
222	Greenland Sea	Mestersvig	72.2N, 23.9W	military base
223	Baffin Bay	Clyde River	70.3N, 68.3W	Indigenous community
224	Hudson Bay	Churchill	58.8N, 94.2W	port, tourism

225



226



227

228 Figure 1. Grid cells (red squares) for which passive-microwave-derived ice concentrations
229 were used in computing the break-up and freeze-up metrics for the coastal locations. Black
230 dots represent the actual locations of the coastal communities. Blue shading denotes
231 maximum (upper panels) and median (lower panels) coverage of landfast ice in June over the
232 1972-2007 period based on charts of the U.S. National Ice Center --
233 <https://nsidc.org/data/G02172> (accessed 28 June 2022).

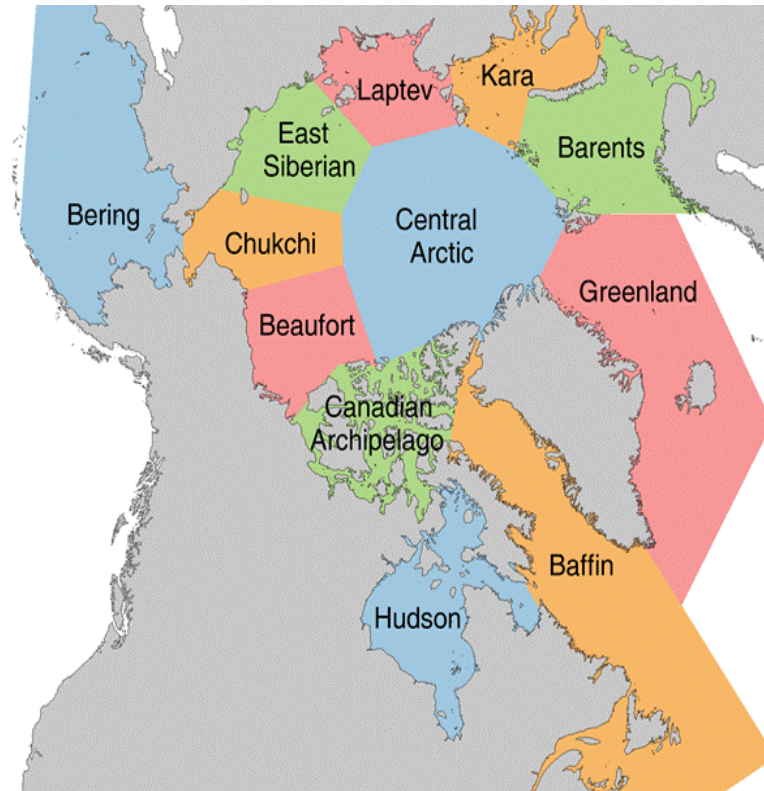
234 It is apparent from Figure 1 that the innermost extent of the landfast ice does not always
235 coincide with the coastline. The northern Siberian coast (Sabetta and Tiksi) provides
236 examples. In pursuing an explanation for the discrepancies, we found that the land mask in the
237 fast ice dataset (digitized charts of the National Ice Center) differs from the land mask of the
238 NSIDC's passive microwave dataset. The resulting offset does not change the area covered by
239 sea ice in each regional plot, but it does result in the mis-location of the nearshore edge. The
240 discrepancy does not alter the reasoning about the geographically varying roles of landfast ice,
241 as discussed in Section 4.

242 The grid cell selections for St. Lawrence Island and the Chukchi Sea deserve special
243 comment. The grid cells off St. Lawrence Island were chosen to reflect timing and location of
244 subsistence harvests by the communities of Gambell and Savoonga. Because of extensive ice
245 coverage, including landfast ice, north and northwest of the island, both communities
246 traditionally conduct bowhead whale harvests at hunting camps on the south side of the island
247 once spring ice break-up is underway (Noongwook et al., 2007). These sites also reflect the
248 seasonal migration of whales in waters south of the island with the seasonal retreat of the ice
249 cover (Noongwook et al., 2007), modulated somewhat by the presence of a polynya south and

250 southwest of the island (Krupnik et al., 2010; Noongwook et al., 2007). Traditional walrus
251 harvest practices on St. Lawrence Island await the very end of the bowhead whale hunt
252 (Kapsch et al., 2010), with timing of spring ice break-up south of the island as the driving
253 factor. These practices motivated our selection of grid cells southeast of the island. As shown
254 later (Section 4), landfast ice is confined to the northern coastal region of St. Lawrence Island
255 – consistent with the frequent presence of the polynya south of the island. In the case of the
256 Chukchi Sea, the grid cells are indeed farther from the coast than for the other sites; the
257 locations were intentionally selected to be farther offshore in order to provide a non-coastal
258 counter-example to the other sites, all of which are adjacent to a coast.

259 Previous studies cited earlier have evaluated break-up and freeze-up metrics for subregions of
260 the Arctic Ocean and the surrounding seas (Markus et al., 2006; Johnson and Eicken, 2016;
261 Bliss and Anderson, 2018; Peng et al., 2018; Bliss et al., 2019; Smith and Jahn, 2019). For
262 comparisons with broader regions offshore of our selected sites, we utilize the MASIE
263 (Multisensor Analyzed Sea Ice Extent) regionalization
264 (https://nsidc.org/data/masie/browse_regions). Of the MASIE regions shown in Figure 2, we
265 choose the following for computation of regionally averaged metrics of break-up and freeze-
266 up: Beaufort Sea, Chukchi Sea, East Siberian Sea, Laptev Sea, Kara Sea, Greenland Sea, (8)
267 Baffin Bay, Hudson Bay, and Bering Sea.

268



269

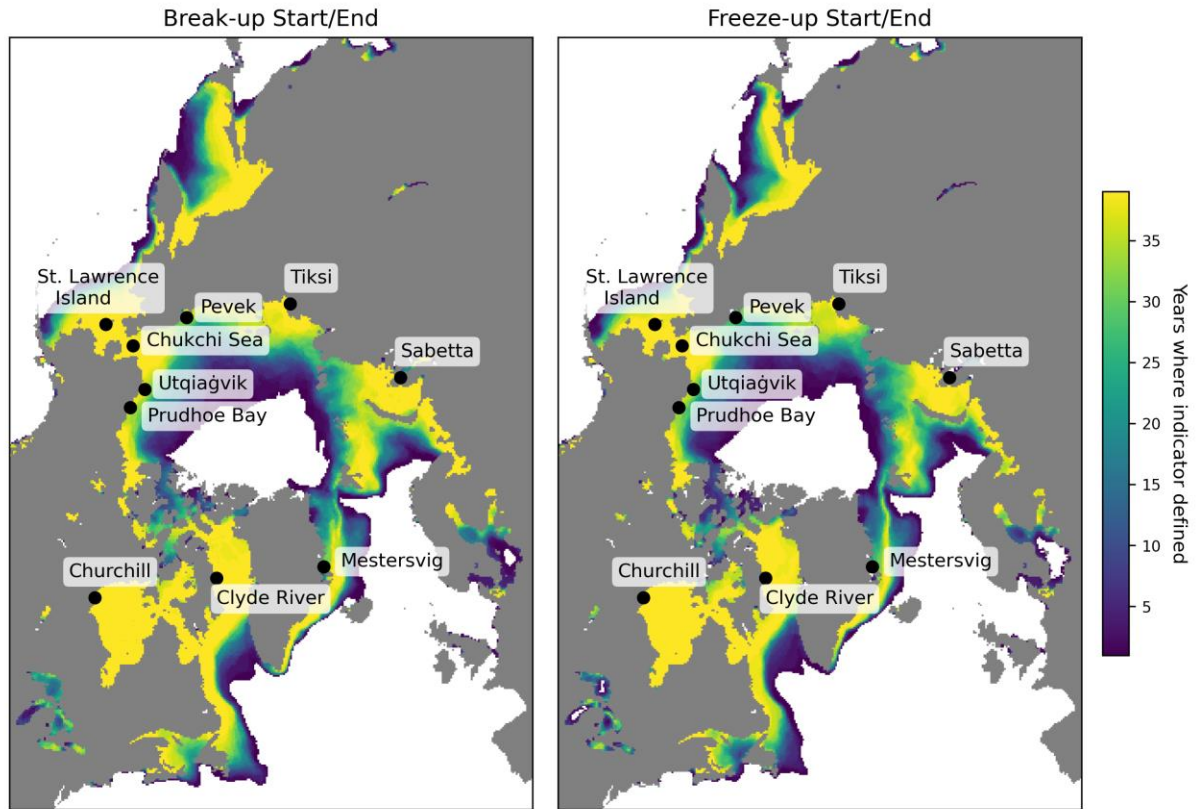
270 Figure 2. The MASIE subregions of the Arctic. Regions utilized in this study include
 271 Beaufort Sea, Chukchi Sea, East Siberian Sea, Laptev Sea, Kara Sea, Baffin Bay, Hudson
 272 Bay, and Bering Sea.

273 The following section includes time series of the local indicators and, for comparison, time
 274 series of the corresponding MASIE regional indicators. In order to address the spatial
 275 coherence of the indicators, we performed a factor analysis on the different sets (break-
 276 up/freeze-up, start/end dates). The computation of the indicators was done for the ten local
 277 sites and for the MASIE regions in which they fall. Factor analysis is a statistical method for
 278 quantifying relationships among a set of variables. The variability in the overall dataset is
 279 depicted by a set of factors. Each factor explains a percentage of the total variance in space
 280 and time. Each variable in each factor is given a loading (or weight) based on its contribution
 281 to the variance explained by that factor. The first factor can be viewed as the linear

282 combination of the variables that maximizes the explained variance in the overall dataset. The
283 second and each successive factor maximize the variance unexplained by the preceding
284 factors. Successive factors explain successively smaller fractions of the overall variance.
285 Multiple variables can have strong loadings in the same factor, indicating they follow a
286 similar pattern and are likely highly related. Factor analysis has a long history of applications
287 to Arctic sea ice variability (Walsh and Johnson, 1982; Fang and Wallace, 1994; Deser et al.,
288 2000; Fu et al., 2021). The factor analysis calculations used here were performed using the
289 XLSAT software package run in Excel (<https://www.xlstat.com/en/>)

290 **3. Results**

291 With coastal ice retreat and onset of ice advance as this study's primary foci, we first
292 demonstrate the applicability of the indicators evaluated here. The various metrics of sea ice
293 break-up and freeze-up in Table 1 are not defined for all locations in the Arctic. For example,
294 locations that remain ice-covered throughout a particular year will not be assigned dates for
295 any of the indicators in that year, and the same is true of locations at which sea ice does not
296 form during a particular year. Figure 3 shows the number of years in the 1979-2018 study
297 period during which the break-up and freeze-up indicators are actually defined. It is apparent
298 that the indicators are consistently defined in the seasonal sea ice zone spanning the subarctic
299 seas. In particular, all ten coastal locations in Table 2 are in the yellow areas (>35 years out of
300 40 years defined) of Figure 3. Of note in Figure 3 is that the number of years with defined
301 break-up indicators slightly exceeds (by one) the number of years with freeze-up indicators at
302 some locations at the outer periphery of the seasonal sea ice zone. These are locations in
303 which sea ice was present for some portion of the early years but not at the end of the study
304 period, so in one of the years there was a break-up but no freeze-up.



305

306 Figure 3. Number of years in the 1979-2018 study period in which the break-up and freeze-up
 307 indicators were defined. Note that end dates for break-up and freeze-up exist only for years in
 308 which there are start dates for break-up and freeze-up. The start and end dates of the overall
 309 data record (1 Jan 1979 – 31 Dec 2018) can result in differences of 1 year in the counts when
 310 freeze-up occurs around January 1.

311 A key issue to be addressed is the degree to which the indicators utilized here differ from
 312 those of previous studies. The metrics of Bliss et al. (2019) or similar variants have been used
 313 in recent publications and provide natural points of comparison. While there are various
 314 differences between our metrics and those of Bliss et al., the most consequential for the
 315 computed dates is the use of departures from winter/summer averages concentrations in our
 316 criteria vs. Bliss et al.'s use of 15% and 80% concentrations as key thresholds. This

317 distinction is analogous to the difference between the NASA Team algorithm's use of fixed
318 tie points and the NASA Bootstrap algorithm's use of "dynamic (time/space-varying) tie
319 points.

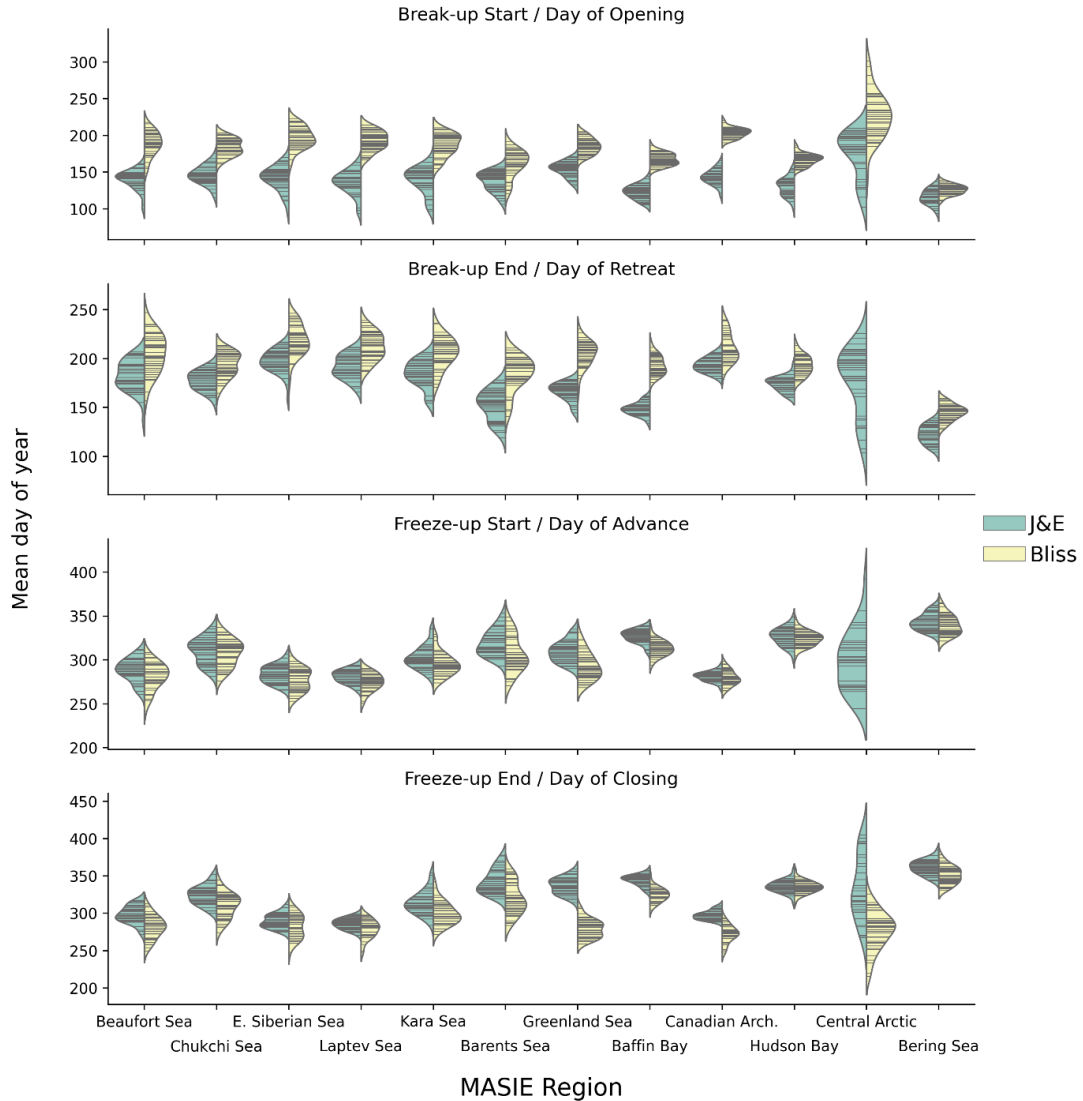
320 The four indicators in this study are the dates of the start and end of break-up and freeze-up.
321 The corresponding indicators used by Bliss et al. (2019) are the date of opening (defined as
322 the last day on which the ice concentration drops below 80% before the summer minimum),
323 the date of retreat (defined as the last day the ice concentration drops below 15% before the
324 summer minimum), the date of advance (defined as the first day the ice concentration
325 increases above 15% following the final summer minimum) and the date of closing (defined
326 as the first day the ice concentration increases above 80% following the final summer
327 minimum). Figure 4 and Table S1 show that there are systematic differences between our
328 metrics (based on J&E) and those of Bliss et al. when the two sets of metrics are evaluated for
329 the MASIE regions. In particular, J&E's start and end of breakup generally occur earlier by
330 up to several weeks than the corresponding dates of opening and retreat defined by Bliss et al.
331 On the other hand, J&E's freeze-up dates are more closely aligned with those of Bliss et al.,
332 although J&E's end-of-freeze-up occurs later (by 1 to 3 weeks) than Bliss et al.'s closing date
333 in most of the MASIE regions, especially the North Atlantic and Canadian regions.

334 The violin plots in Figure 4 show distributions but not the temporal variations that have been
335 indicated by results of previous studies (Peng et al., 2018; Bliss et al., 2019). Figures 5 and 6
336 provide the temporal perspective on the end dates of break-up (Day of retreat) and freeze-up
337 (Day of closing), respectively. In each of the MASIE regions, the J&E criterion gives an
338 earlier break-up date. The difference is typically two to three weeks, although it exceeds a
339 month in the Greenland Sea and Baffin Bay. Despite the offsets, the trends are nearly the

340 same in nearly all the regions. Exceptions are the Canadian Archipelago, where the J&E trend
341 is weaker than the Bliss trend, and the Bering Sea, where the trends are opposite in sign.
342 However, the trend in the Bering region is not statistically significant at the 99% level by
343 either metric, in contrast to all other regions in which the trends are significant at this level
344 (Table S2). The main conclusion from Figure 5 is that, except for the Bering Sea, sea ice
345 break-up is occurring earlier throughout the Arctic than several decades ago, no matter which
346 metric is used.

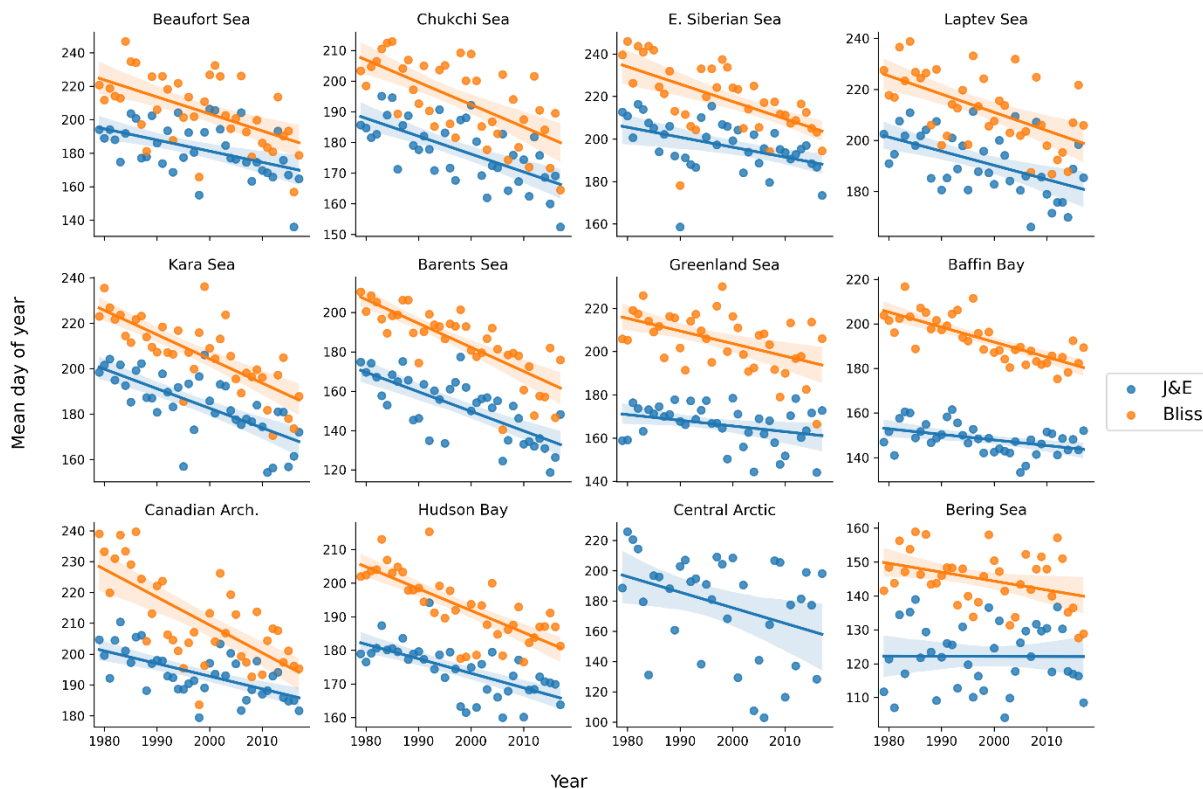
347 In contrast to the trends towards earlier breakup, the J&E and Bliss metrics for the end of
348 freeze-up both show significant trends towards later dates in most of the MASIE regions
349 (Figure 6 and Table S3). In this case, even the Bering Sea shows a trend towards later freeze-
350 up. Again, there is an offset towards a later date with the J&E metric, although the offset has
351 a range among the regions, from essentially zero in Hudson Bay to more than six weeks in the
352 Greenland Sea. The trends, however, show less agreement in some regions than do the trends
353 for break-up dates in Figure 5. The J&E trends are more strongly positive in the seas of the
354 eastern Russian sector: the Chukchi, East Siberian and Laptev Seas. The same is true,
355 although to a lesser degree, in the Barents Sea and the Canadian Archipelago. The main
356 message from Figure 6 is that the freeze-up is ending later throughout the Arctic, although the
357 magnitude of the trend is more sensitive to the criteria used for end-of-freeze-up than for end-
358 of-break-up.

359



360

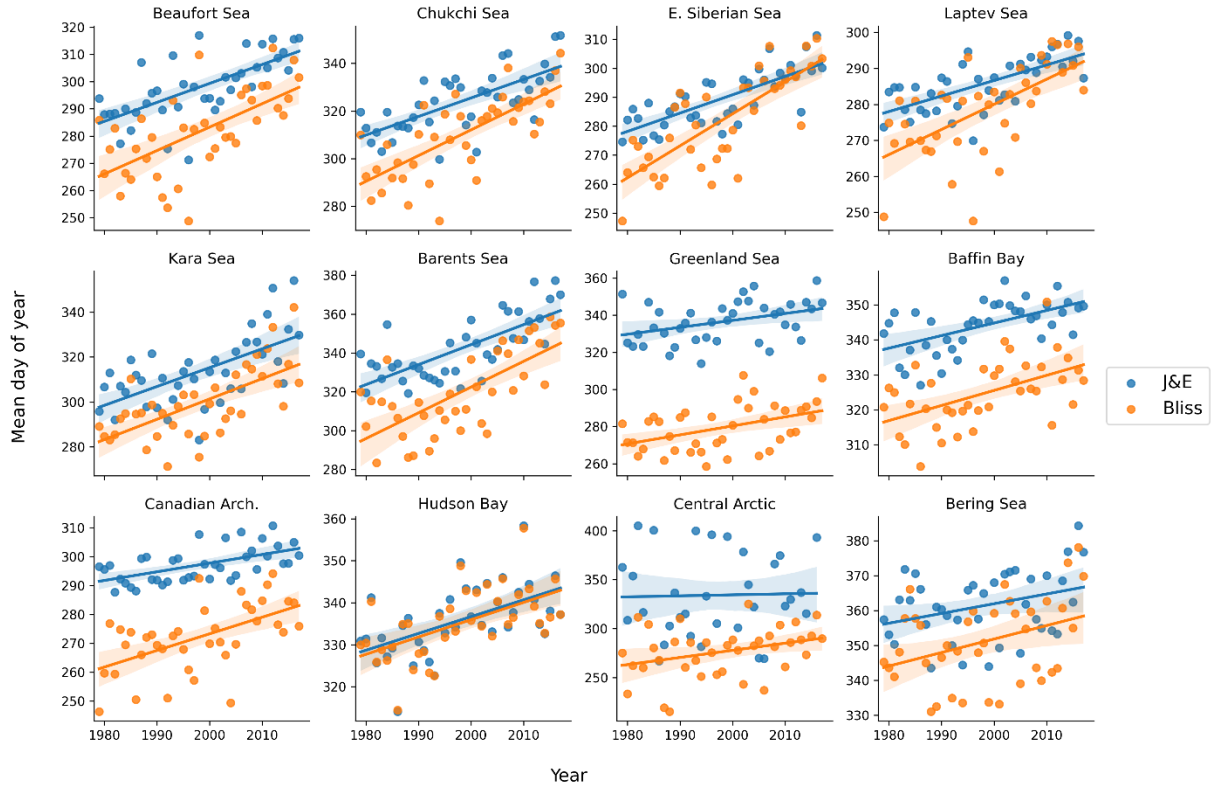
361 Figure 4. “Violin” plots of the Julian dates of the break-up/freeze-up metrics used in this
 362 study based on Johnson and Eicken (2016) (green shading) and the corresponding dates of ice
 363 opening, retreat, advance and closing as defined by Bliss et al. (2019) (yellow shading). A
 364 violin plot shows a distribution by widening the horizontal lines in the ranges (of day of the
 365 year, in this case) having the highest concentration of values. The thin black lines represent
 366 the observations themselves; the black strips are clusters of lines representing groups of
 367 similar values in the distribution. The violin plots provide no information about the temporal
 368 sequence of the values.



370

371 Figure 5. Yearly values of J&E's break-up end date (blue symbols) and the Bliss et al.'s
 372 (2019) Day of retreat (orange symbols) in the various MASIE regions. Corresponding trend
 373 lines are shown in each panel. (For the Central Arctic region, the Bliss metric (Day of retreat)
 374 was not defined for a sufficient number of years). Y-axis labels represent day of the year. Date
 375 scales on y-axis vary among panels in order to optimize display of data points. Numerical
 376 values of slopes and their significance levels are provided in Table S2.

377



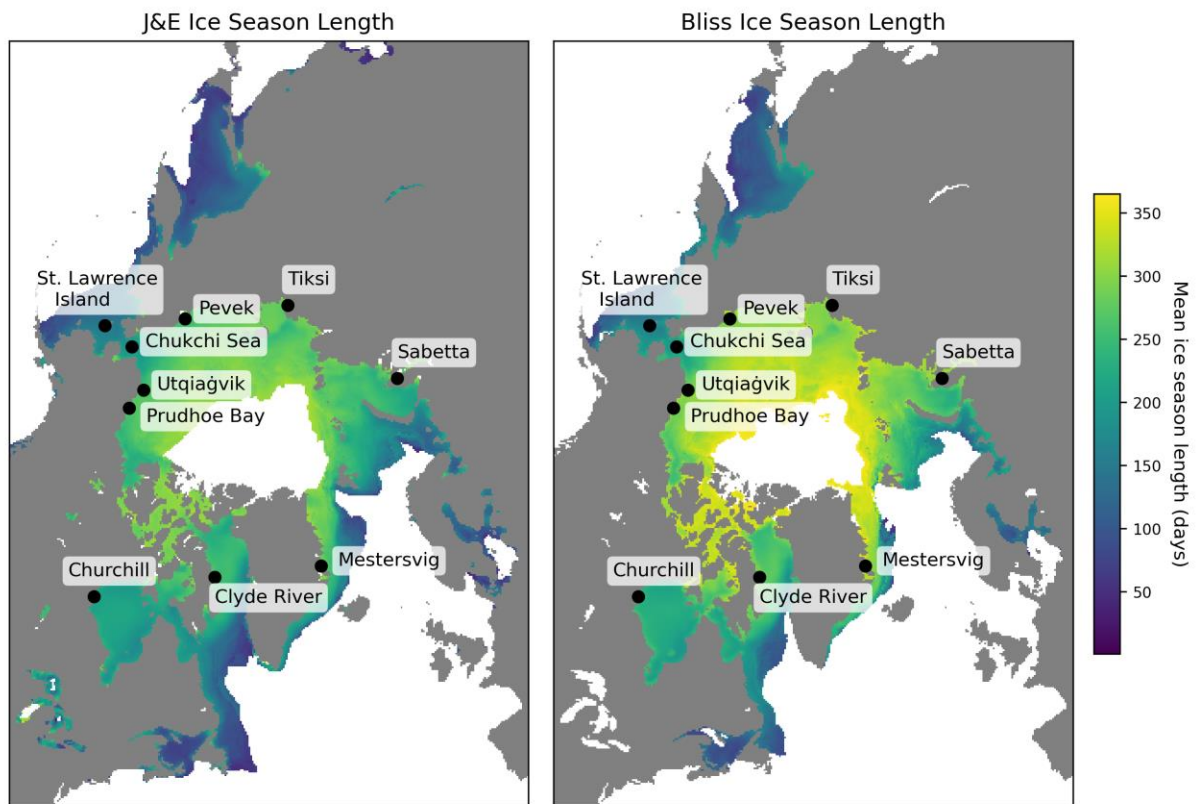
378

379 Figure 6. Yearly values of J&E’s freeze-up end date (blue symbols) and the Bliss et al.’s
 380 (2019) Day of closing (orange symbols) in the various MASIE regions. Corresponding trend
 381 lines are shown in each panel. Y-axes labels represent day of the year. Date scales on y-axis
 382 vary among panels in order to optimize display of data points. Numerical values of slopes and
 383 their significance levels are provided in Table S3.

384

385 A final comparison is presented in Figure 7, which shows the ice season lengths computed
 386 using the two sets of metrics. The ice season length is defined as the number of days between
 387 the end of freeze-up and the start of break-up. Consistent with J&E’s earlier break-up (Figure
 388 5) and later freeze-up (Figure 6), the J&E metrics yield a shorter ice season than the Bliss et al
 389 metrics. The differences in Figure 7 exceed a month in most of the Arctic except for the

390 Bering Sea, Hudson Bay and the Canadian Archipelago. However, the negative trends of ice
391 season length are similar in magnitude according to both sets of metrics over most of the
392 Arctic. The trend maps are not shown here because they add little to the information conveyed
393 in Figures 5 and 6.



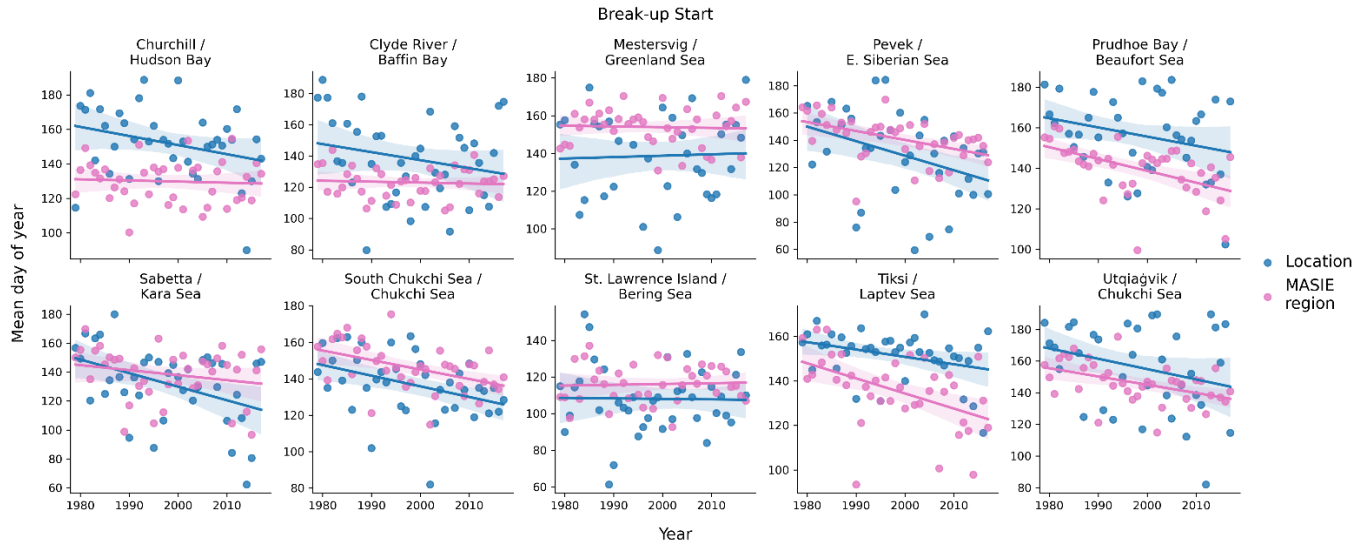
394
395 Figure 7. Mean ice season length based on the J&E metrics (left) and the Bliss et al. (2019)
396 metrics (right). Metrics of break-up and freeze-up were not defined in a sufficient number of
397 years in the white area near the North Pole.

398 Given that the development of local indicators is a main objective of this study, it is important
399 to assess the relationship between the local indicators and those for the broader MASIE
400 regions containing the coastal locations. Figures 8-11 provide these comparisons for all four

401 metrics defined by the modified J&E algorithms. In all cases, the yearly values (and linear
402 trend lines) for the ten coastal locations in Table 3 are plotted for the 1979-2018 period,
403 together with the values for the corresponding MASIE regions.

404 The break-up start dates (Figure 8) differ between the coastal locations and the broader
405 MASIE regions in most of the ten cases, and in some cases the trends are notably different.
406 With regard to systematic differences, not only the magnitude but also the sign of the offsets
407 varies among the regions. The break-up start date at the coast is later than for the MASIE
408 regions for Prudhoe (Beaufort Sea), Utqiagvik (Chukchi Sea), Tiksi (Laptev Sea), and both
409 Canadian locations: Churchill (Hudson Bay) and Clyde River (Baffin Bay). These sites are all
410 Arctic coastal locations at which varying extents of landfast ice are present. By contrast, the
411 coastal locations have earlier break-up start dates (relative to their corresponding MASIE
412 regions) at St. Lawrence Island (Bering Sea), Mestersvig (Greenland Sea) and the Bering
413 Strait (Chukchi Sea). These locations are less prone to experience a buildup of landfast ice
414 during the winter. The results imply that landfast ice plays a role in the timing of the start of
415 breakup at coastal locations relative to the broader sector of the seasonal sea ice zone. The
416 processes by which landfast ice affects the timing of break-up are discussed in Section 4.

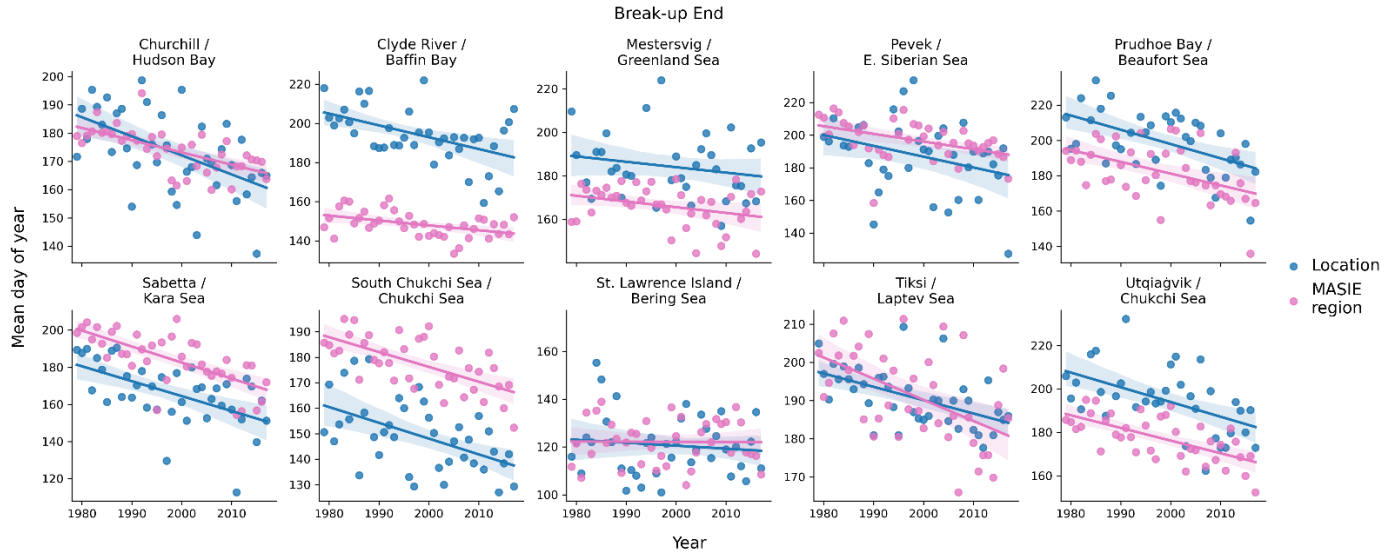
417 While the general trend towards earlier break-up noted above (Figure 5) is apparent at most of
418 the coastal locations, the magnitudes of the trends can differ between the coastal sites and the
419 broader MASIE regions. Figure 8 shows that the trend towards an earlier start of break-up is
420 stronger at the coastal location relative to the MASIE region at Churchill, Clyde River, Pevek
421 and Sabetta. Only at Tiksi is the negative trend weaker at the coastal site. In the other regions
422 the trends are nearly identical.



423

424 Figure 8. Yearly values (1979-2018) of the break-up start dates (shown as day-of-the-year
 425 numbers) for the coastal locations (blue) and the corresponding MASIE regions (purple). Date
 426 scales on y-axis vary among panels in order to optimize display of data points. Linear regression
 427 lines are shown with the same color coding. In each panel, the upper line of header identifies the
 428 coastal location and the lower line identifies the MASIE region. All values are based on the
 429 modified J&E algorithms. Slopes and their significance levels are listed in Tables S2 and S3.

430 The break-up end dates (Figure 9) show differences similar to those in Figure 8 in most, but not
 431 all, cases. The break-up end date occurs earlier at Clyde River, Prudhoe and Utqiagvik relative
 432 to the MASIE regions, as is the case with the results in Figure 8. However, unlike the break-up
 433 start date, the break-up end date also occurs earlier at Mestersvig than for the Greenland Sea
 434 MASIE region. The opposite relationship is found in the Kara Sea / Sabetta and the Chukchi
 435 Sea (Bering Strait), where the MASIE region has the earlier break-up end date. The temporal
 436 trends in the break-up end dates are generally similar for the coastal locations and the MASIE
 437 regions, and there are no differences in sign. All coastal locations and all MASIE regions show
 438 negative trends, i.e., trends toward earlier break-up end dates in recent decades.



439

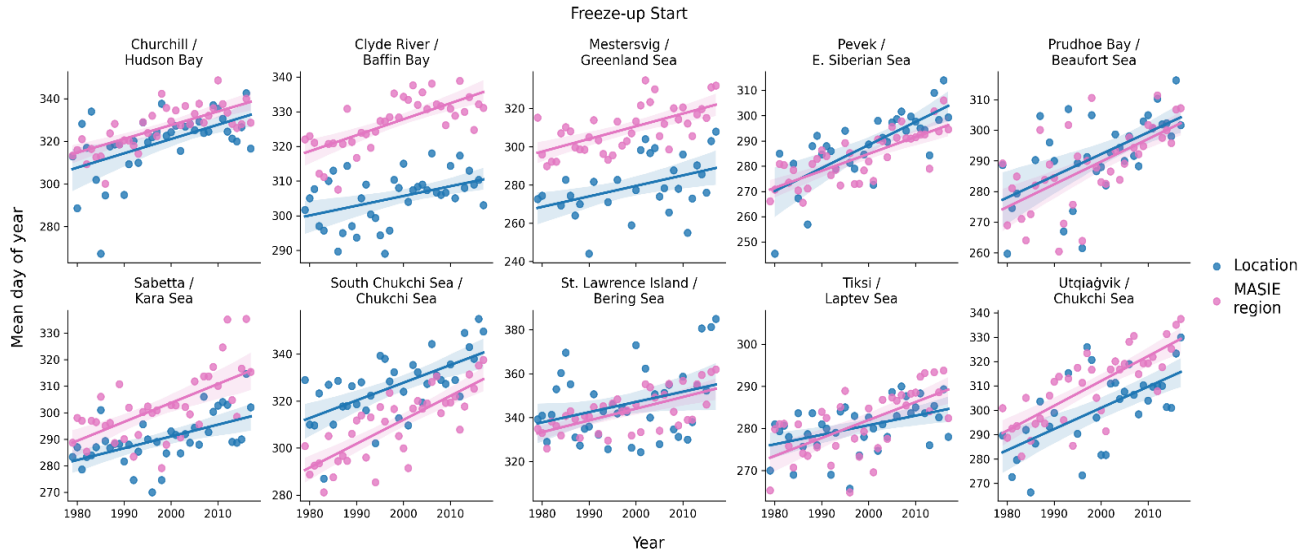
440 Figure 9. Yearly values (1979-2018) of the break-up end dates (shown as day-of-the-year
 441 numbers) for the coastal locations (blue) and the corresponding MASIE regions (purple). Date
 442 scales on y-axis vary among panels in order to optimize display of data points. Linear
 443 regression lines are shown with the same color coding. In each panel, the upper line of header
 444 identifies the coastal location and the lower line identifies the MASIE region. All values are
 445 based on the modified J&E algorithms. Slopes and their significance levels are listed in Tables
 446 S2 and S3.

447 The freeze-up start dates are compared in Figure 10. Several regions show large offsets, most
 448 notably Clyde River (Baffin Bay) and Mestersvig (Greenland Sea), where the start of freeze-
 449 up occurs earlier at the coast by several weeks. Both Baffin Bay and the Greenland Sea are
 450 large MASIE regions (Figure 2), favoring the delay of freeze-up start
 451 portion of the seasonal sea ice zone within the respective MASIE regions. Freeze-up start
 452 dates are also earlier than offshore at several other coastal locations: Churchill, Sabetta and
 453 Utqiagvik. These are regions in which it is common for ice to form along the coast in autumn,

454 with the ice edge advancing offshore to meet the expanding main ice pack as freeze-up
455 progresses. By contrast, the southern Chukchi Sea location has a later freeze-up date than the
456 Chukchi MASIE region, largely because the southern Chukchi grid cells are located in an area
457 of relatively warm inflowing currents from the Bering Sea and are in the southern portion of
458 the Chukchi MASIE region. As with the break-up end dates, all coastal locations and MASIE
459 regions show trends of the same sign. In this case, the trends are all positive, indicating a later
460 start to freeze-up.

461 Finally, Figure 11 compares the freeze-up end dates for the ten coastal sites and their MASIE
462 regions. The results are quite similar to those for the freeze-up start dates in Figure 10.
463 Relative to the MASIE regions as a whole, freeze-up ends earlier at both Canadian sites
464 (Churchill and Clyde River), Mestersvig, Sabetta and Utqiaġvik. Again, the differences are
465 especially large (more than a month) at Clyde River and Mestersvig, both of which are in
466 large MASIE regions as noted above. The southern Chukchi Sea and, to a lesser extent in
467 recent decades, Pevek (East Siberian Sea) show later freeze-ups near the coast than for the
468 MASIE region. Once again, all trends are positive, pointing to a later end to freeze-up at
469 coastal as well as offshore regions throughout the Arctic. The changes in the freeze-up dates
470 over the 40-year period are especially large, exceeding one month, at Pevek (East Siberian
471 Sea) and Prudhoe (Beaufort Sea). The changes are close to a month at Utqiaġvik (Chukchi
472 Sea) and the Southern Chukchi Sea.

473

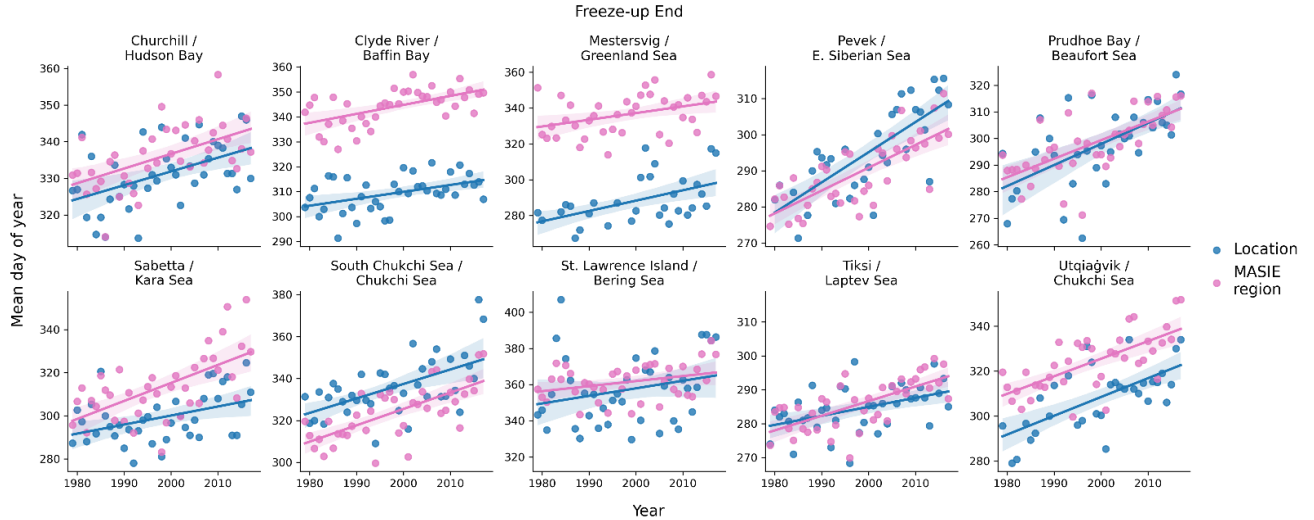


474

475 Figure 10. Yearly values (1979-2018) of the freeze-up start dates (shown as day-of-the-year
 476 numbers) for the coastal locations (blue) and the corresponding MASIE regions (purple). Date
 477 scales on y-axis vary among panels in order to optimize display of data points. Linear
 478 regression lines are shown with the same color coding. In each panel, the upper line of header
 479 identifies the coastal location and the lower line identifies the MASIE region. All values are
 480 based on the modified J&E algorithms. Slopes and their significance levels are listed in Tables
 481 S2 and S3.

482

483



484

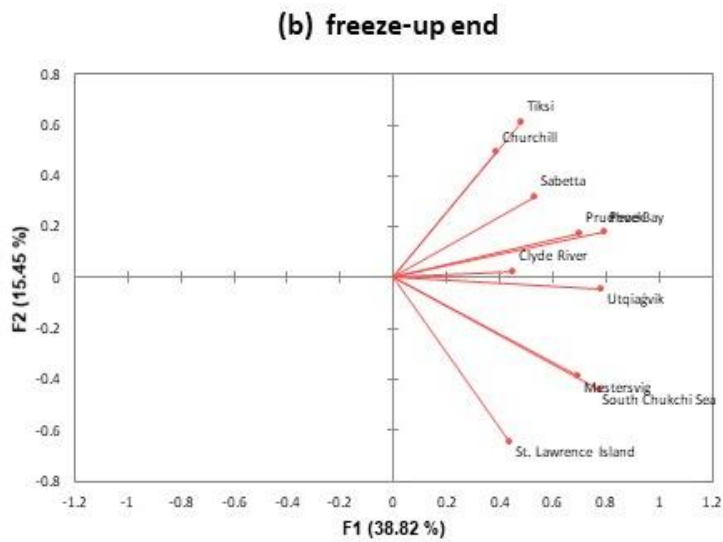
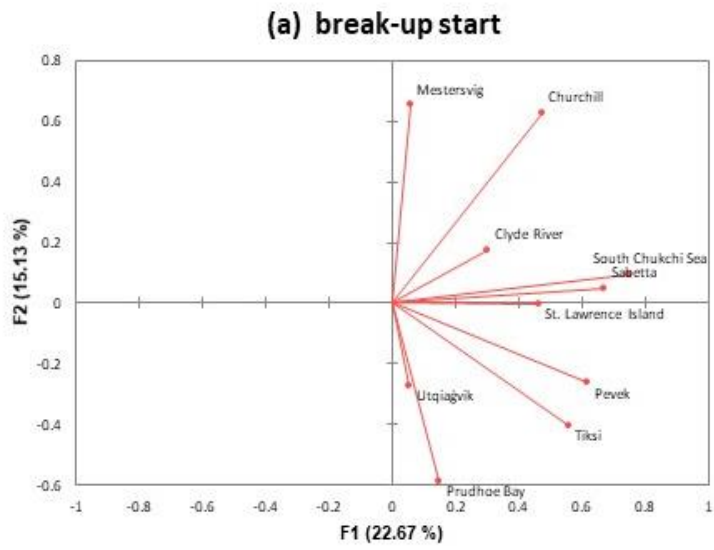
485 Figure 11. Yearly values (1979-2018) of the freeze-up dates (shown as day-of-the-year
 486 numbers) for the coastal locations (blue) and the corresponding MASIE regions (purple). Date
 487 scales on y-axis vary among panels in order to optimize display of data points. Linear
 488 regression lines are shown with the same color coding. In each panel, the upper line of header
 489 identifies the coastal location and the lower line identifies the MASIE region. All values are
 490 based on the modified J&E algorithms. Slopes and their significance levels are listed in Tables
 491 S2 and S3.

492 In order to synthesize the information provided by the local indicators, we applied a factor
 493 analysis to each of the four local indicators described in Section 2. For the local indicators,
 494 each input matrix was 10 (locations) x 40 (years). For comparison, we also applied the factor
 495 analysis to the corresponding regional sea ice areas from the MASIE database (National Snow
 496 and Ice Data Center dataset G02135_v3.0-4). Because the Chukchi Sea is the MASIE region
 497 for two of the local indicators (Chukchi Sea and Utqiagvik), the data matrix for the MASIE
 498 regional factor analysis contained 9 (regions) x 40 (years) entries. We performed the MASIE

499 factors separately for middle months of the break-up and freeze-up seasons (June and
500 November, respectively).

501 In all cases, the first factor contains loadings of the same sign for all locations/regions and is
502 essentially a depiction of the temporal trends, which account for substantial percentages of the
503 variance. The second factor consists of loadings of both signs, corresponding to positive
504 departures from the mean at some locations and negative departures at others. Figure 12
505 illustrates this behavior for (a) the break-up start dates and (b) the freeze-up end dates. While
506 every one of the ten locations has a positive loading in Factor 1, the mixed signs of the Factor
507 2 loadings point to a regional clustering of the dates. For example, Figure 12a shows that the
508 northern coastal sites in the Pacific hemisphere (Prudhoe Bay, Utqiagvik, Tiksi, Pevek) have a
509 component of break-up start date variability that is out of phase with the locations in the
510 western Atlantic/eastern Canada sector (Mestersvig, Churchill, Clyde River).

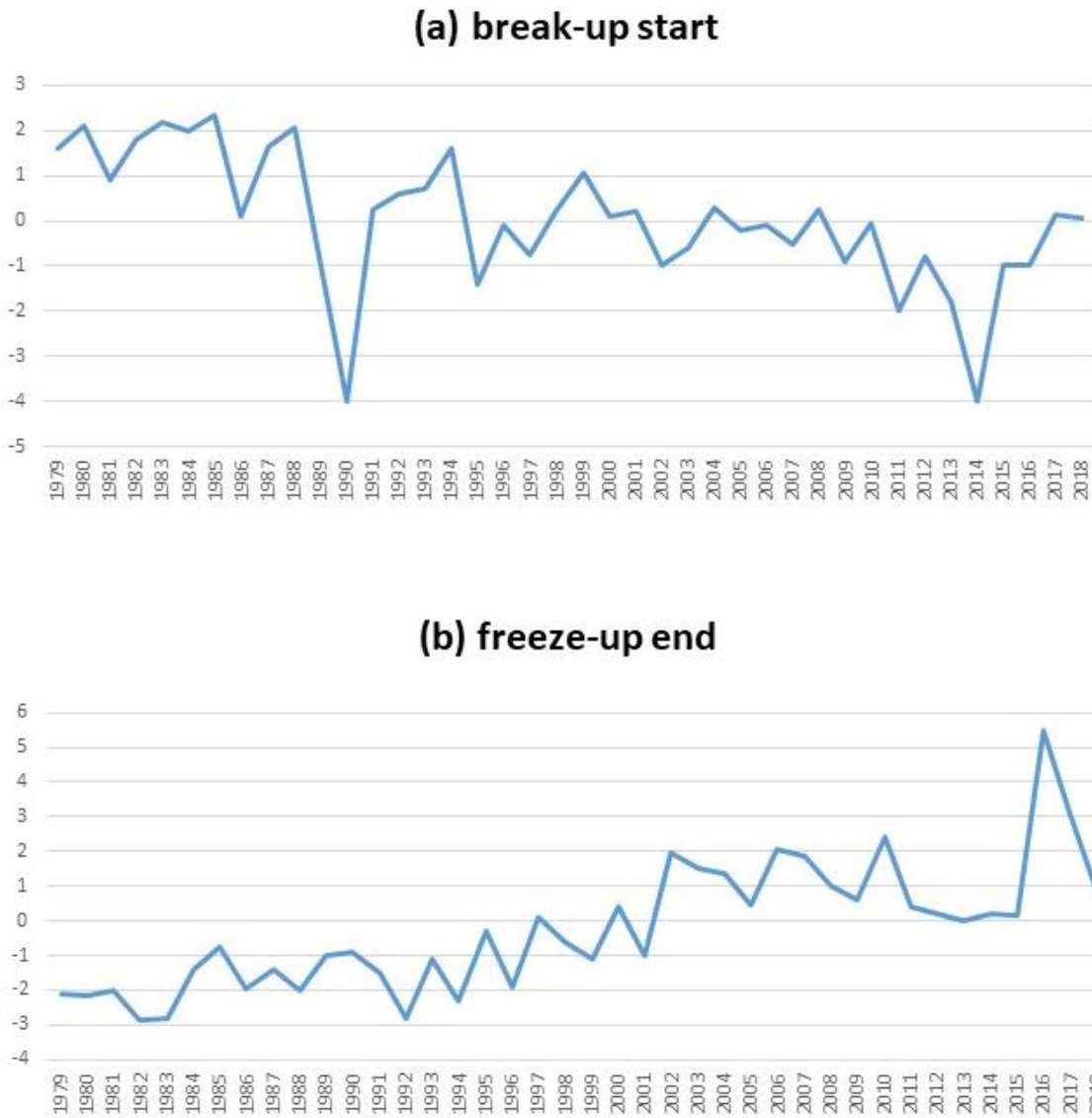
511 The interpretation of Factor 1 as a trend mode is supported by Figure 13, which shows the
512 time series of the scores of Factor 1 for (a) the break-up start date and (b) freeze-up end dates.
513 The trends towards an earlier start of break-up and a later end of freeze-up are clearly evident.
514 Figure 13 also illustrates the tendency for occasional “outlier” years to be followed by a
515 recovery in the following year. These plots and those for the other local indicators show that
516 these extreme excursions and recoveries are superimposed on the strong underlying trends,
517 resulting in new extremes when the sign of an extreme year is the same as the sign of the
518 underlying trend.



519

520 Figure 12. Loadings for Factor 1 (x-axis) and Factor 2 (y-axis) for (a) the start of break-up and (b)
 521 the end of freeze-up at the ten local coastal sites. Labels on vectors denote locations.

522



523

524 Figure 13. Scores (time series) for Factor 1 of (a) the start of break-up and (b) the end of
 525 freeze-up at the ten local coastal sites.

526 Table 4 shows that the first two factors explained more than half the variance for all local and
 527 MASIE indicators except the local break-up start date. The break-up start date is notable for
 528 the small percentages of variance explained by the first two factors. The implication is that
 529 local conditions play a relatively greater role in the timing of the start of break-up. These local

530 factors can include landfast ice, inflow of water and heat from the adjacent land areas
531 (including rivers), and possibly other effects related to local ocean currents or local weather
532 conditions. The freeze-up start date has the most spatial coherence in the trend mode (55.7%
533 of the explained variance). However, as shown by the last two lines of Table 4, the MASIE
534 regional ice areas have even greater percentages of variance explained by the first two factors.
535 In both the break-up and freeze-up seasons (June and November), the first two factors explain
536 more than 60% of the variance (vs. 37.8%-55.7% for the local indicators). Because the
537 variance of the ice concentrations in the MASIE regions is generally greater in the southern
538 compared to the northern portion of the region, factors for individual MASIE regions have
539 greater loadings in the south. However, this does not provide an obvious explanation for why
540 the percentage of variance explained by the first factor is greater for the MASIE indicators
541 than for the local indicators. These differences again point to the importance of local
542 conditions relative to the broader underlying trend in ice coverage, as Factor 1 (the trend)
543 accounts for most of the differences between the local and regional results in Table 4.

544

545 Table 4. Percentages of variance explained by Factors 1 and 2. Numbers in parentheses are
546 the contributions of the individual factors (Factor 1 + Factor 2).

547

548	Break-up start (local)	37.8%	(22.7% + 15.1%)
549	Break-up end (local)	50.9%	(37.6% + 13.3%)
550	Freeze-up start (local)	55.7%	(40.1% + 15.6%)
551	Freeze-up end (local)	54.3%	(38.8% + 15.5%)

552

553 MASIE ice areas: June 60.9% (47.1% + 13.8%)

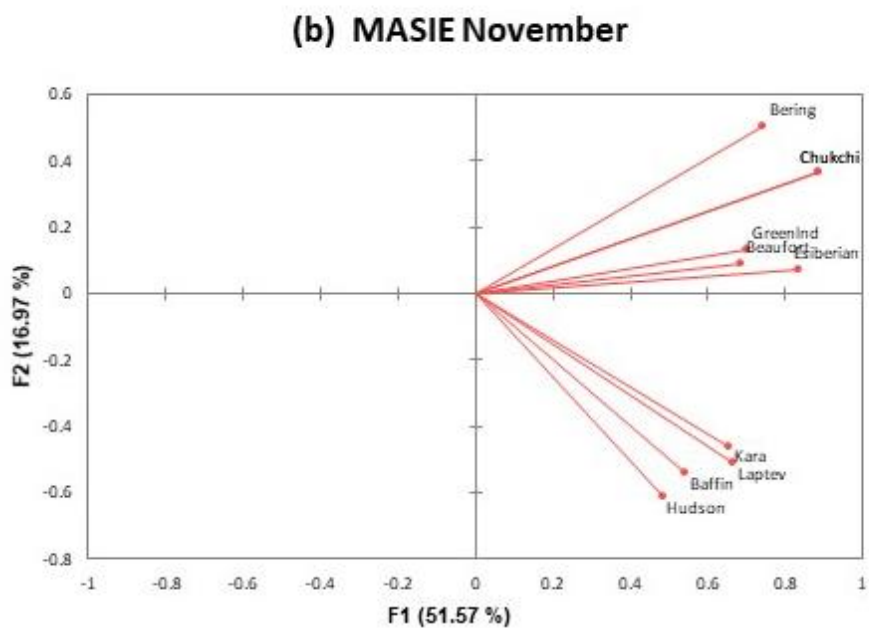
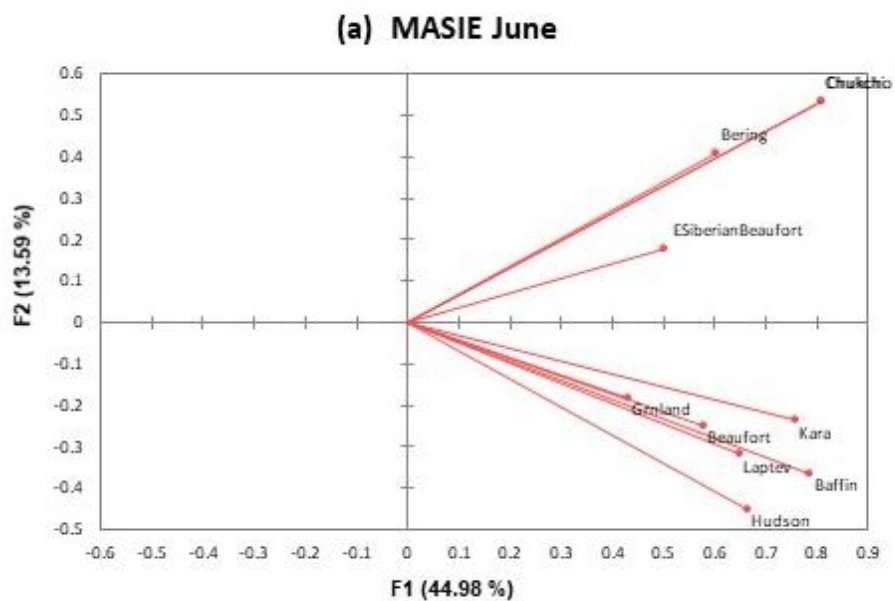
554 MASIE ice areas: November 64.1% (48.7% + 15.4%)

555

556 Finally, Figure 14 illustrates the tendency for tighter clustering in the regional indicators. For
557 both the June and November results, the clustering in Figure 14 is clearly more distinct than in
558 Figure 12, which is the corresponding figure for the local indicators. The clustering in Figure
559 14 is geographically coherent, e.g., the Pacific sector sites (Bering, Chukchi, East Siberian)
560 are in a distinct cluster for the June (break-up), while subclusters for November include the
561 Hudson and Baffin regions, the Kara and Laptev regions, and the Bering and Chukchi regions.
562 The results imply that underlying trends and spatially coherent patterns of forcing will be
563 more useful in explaining – and ultimately predicting – variations of regional sea ice cover.
564 However, diagnosis and prediction of local indicators will require a greater reliance on
565 additional information such as local geography and local knowledge, including information
566 from residents and other stakeholders who have had experience with break-up and freeze-up
567 of sea ice in the immediate area.

568

569



570

571 Figure 14. Loadings for Factor 1 (x-axis) and Factor 2 (y-axis) for the MASIE regional ice
 572 areas of (a) June and (b) November. Labels on vectors denote MASIE regions.

573

574 4. Discussion

575 The results presented in Section 3 point to a lengthening of the open water season as a result
576 of both an earlier break-up and a later freeze-up. The timing of break-up and freeze-up relates
577 to the proximity to the coast. In this section, we first place the trends obtained here in the
578 context of past studies. We then address the distinct characteristics of the near-coastal waters
579 by discussing landfast ice and its role in break-up and freeze-up, again drawing upon the
580 published literature for context.

581 The lengthening of the open-water season in the Arctic has been well-documented (e.g.,
582 Stroeve et al., 2014; Stroeve and Notz, 2018; Onarheim et al., 2018; Bliss and Anderson,
583 2018; Peng et al., 2019; Smith and Jahn, 2019). As a result, the percentage of the Arctic sea
584 ice cover experiencing break-up and freeze-up (i.e., the percentage of the maximum ice cover
585 that is seasonal) has increased from about 50% in 1980 to more than 70% in recent years
586 (Druckenmiller et al., 2021; Thomson et al., 2022). Since 1980, the length of the open water
587 period has increased by between one and two months (over 10 days per decade)
588 (Stammerjohn et al., 2012; Peng et al., 2019; Thomson et al., 2022), with contributions of
589 comparable magnitude from earlier break-up and later freeze-up. Regional variations of these
590 trends, both in the vicinity of the coasts and in regions farther offshore, are the focus of this
591 paper as well as Bliss et al. (2019), to which we have compared our results.

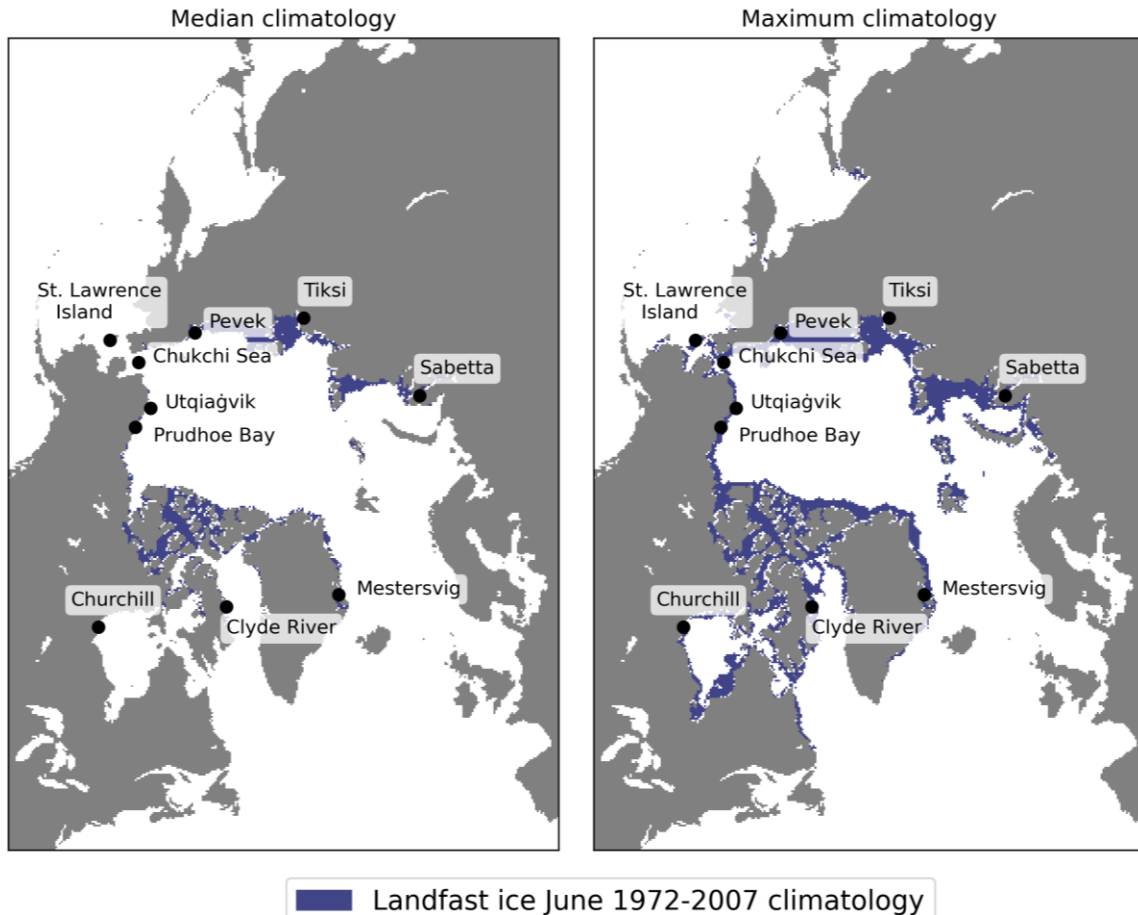
592 Trends in freeze-up have been shown previously to be sensitive to the criterion for freeze-up
593 (Peng et al., 2018; Bliss et al., 2019). For example, Peng et al. (2018) found that the trends in
594 the autumn crossing of the 80% concentration were greater than trends in the crossing of the
595 15% threshold (Thomson et al., 2022), implying a slowing of the autumn/winter ice advance.

596 Such findings, as well as those of Johnson and Eicken (2016), have motivated our use of
597 separate indicators for the start and end of break-up and freeze-up.

598 The delayed autumn freeze-up is a manifestation of the release of increased amounts of heat
599 stored in the upper layers of the ocean, largely as a result of the increased solar absorption
600 made possible by the earlier break-up. In this respect, trends in break-up and freeze-up are
601 intertwined. This linkage has been demonstrated quantitatively by Serreze et al. (2016) and
602 Stroeve et al. (2016), who explored the use of break-up timing as a predictor of the timing of
603 ice advance in the Chukchi Sea and the broader Arctic, respectively.

604 The results in Section 3 show that the timing of break-up differs at coastal and offshore
605 locations. In most cases, these differences can be related to the presence of landfast ice, which
606 characterizes the nearshore coastal waters to varying degrees at most of our coastal sites.
607 Figure 15 shows the median and maximum extent of landfast ice during June for the period
608 1972-2007. Landfast ice is most extensive over shallow waters of the Siberian Seas and the
609 Canadian Archipelago, although it can develop in the general vicinity of all of our sites (Fig.
610 1), with the exception of the offshore location in the Chukchi Sea. Given its widespread
611 presence at the coastal sites in the Arctic, landfast ice a key feature in our assessment of
612 coastal-offshore differences in particular for ice break-up. It is for this reason that we have
613 attempted to place our findings into a context of landfast ice.

614



615

616 Figure 15. Landfast ice climatology for June based on the digitized ice charts of the National
 617 Ice Center. Blue shading denotes median extent (left panel) and maximum extent (right
 618 panel) of landfast ice over the 1972-2007 period. Data source: National Ice Center via
 619 National Snow and Ice Data Center, NSIDC dataset G02172 -- <https://nsidc.org/data/G02172>
 620 (accessed 28 June 2022).

621

622 Landfast ice generally persists longer than pack ice in the adjacent offshore in spring. This
 623 contrast can be explained largely in terms of the stationary nature of the landfast ice cover,
 624 with grounded pressure ridges and confinement by coastal barrier islands (e.g., in the Beaufort
 625 and Kara Seas) locking the ice cover in place. Differences in ice thickness, with offshore sea

626 ice younger and hence thinner in areas of coastal polynyas with winter new-ice formation
627 (e.g., in the Chukchi, Beaufort and Laptev Seas) may also contribute to longer persistence of
628 landfast ice. Finally, with thermal decay of sea ice as a key break-up mode, the absorption of
629 solar shortwave energy in leads and openings in the offshore ice pack promotes thinning and
630 decay of the offshore ice relative to that of the landfast ice. The latter is mostly lacking such
631 areas of open water, rendering lateral melt and ocean-to-ice heat transfer from subsurface
632 ocean heat storage less effective (see also Petrich et al., 2012).

633 For coastal sites situated partly or wholly within a landfast ice zone, the breakup dates
634 described in Section 3 are highly dependent on the break-up of the landfast ice. Petrich et al.
635 (2012) describe two dominant break-up modes for landfast ice. Dynamic or mechanical
636 break-up occurs when the action of the wind, ocean swell or currents, and variations in
637 sealevel height promote weakening of the ice cover, detachment from the seafloor and
638 advection of the ice away from the coast. Thermal breakup results from surface and bottom
639 ablation and internal melt, aided further by formation of surface melt ponds. Dispersion is not
640 required for thermal breakup. As noted by Petrich et al. (2012), the mode of ice breakup is
641 often determined by the extent of grounded pressure ridges.

642 In the autumn, water in the shallow coastal areas cools more rapidly to the freezing point
643 because there is less stored heat below the surface. Coastal waters can also be fresher than
644 offshore waters because of terrestrial runoff that freshens the nearshore areas during the warm
645 season. Under such conditions both a higher freezing point and reduction of convective
646 overturning promote earlier freeze-up (Dmitrenko et al., 1999). As a result, the autumn freeze-
647 up often proceeds outward from the coast as well as shoreward from the main pack ice
648 (Thomson et al., 2022, their Fig. 4). However, onset of freeze-up – and depending on the

649 geographic setting and offshore ocean and atmosphere conditions potentially also end of
650 freeze-up – do not correspond with onset of landfast ice formation. In the Chukchi and
651 Beaufort Sea, first appearance of landfast ice may lag freeze onset by a couple of weeks to
652 three months (Mahoney et al., 2014). In more sheltered and less dynamic environments such
653 as the Laptev Sea, inshore landfast ice typically does not form for another couple of weeks
654 after onset of freeze-up and generally takes more than a month to extend further offshore
655 (Selyuzhenok et al., 2015). Hence, freeze-up variability and trends reported in this study are
656 seen as largely independent of landfast ice processes.

657 Conversely, timing of freeze-up does impact the seasonal evolution of landfast ice. Mahoney
658 et al. (2007) discuss mean climatology of annual landfast ice from 1996-2004, including
659 analyses of the maximum, minimum and mean extents. Notable for the results presented in
660 the present study is Mahoney et al.'s finding of a reduced presence of landfast ice in Beaufort-
661 Chukchi region, due to later formation and earlier breakup. In a follow-up study, Mahoney et
662 al. (2014) addressed the geographical variability of break-up and freeze-up, especially as it
663 relates to landfast ice. Their results show that landfast ice in the central and western Beaufort
664 Sea forms earlier, breaks up later, occupies deeper water and extends further from shore than
665 that in the Chukchi Sea. These differences are partially due to the orientation of the coastline
666 relative to the prevailing easterly winds, which can more readily advect ice away from the
667 southwest-northeast oriented coastline of the Chukchi Sea. Hosekova et al. (2021) examined
668 landfast ice along the northern Alaska coast in the context of the buffering of the coastline
669 from wave activity. They found that the wave attenuation by landfast ice was weaker in
670 autumn than in spring because of the lower ice thickness in autumn compared to spring.
671 However, the importance of waves for breakup is somewhat limited because it typically

672 requires large fetch with does not develop until later in the summer and fall, well past the end
673 of break-up season.

674 Yu et al. (2014) showed that landfast ice has large interannual variations, which imply large
675 variations in break-up and freeze-up. Superimposed on these variations were notable trends in
676 landfast ice during Yu et al.'s study period, 1976-2007. More specifically, the duration of
677 landfast ice was found to have shortened in the Chukchi, East Siberian and Laptev Seas,
678 primarily as a result of a slower offshore expansion of landfast ice during the autumn and
679 early sinter since 1990. Our coastal sites in these sectors (Utqiagvik, Pevek and Tiksi) show
680 notable trends toward earlier break-up and later freeze-up, consistent with Yu et al.'s (2014)
681 trends in landfast ice.

682
683 Cooley et al. (2020) examined the sensitivity of landfast ice break-up at the community level
684 in the Canadian Arctic and western Greenland to temperature variations and trends based on
685 analysis of visible satellite imagery. Our analysis provides a longer reference period (40 years
686 vs. 19 years) and a broader geographical context for the work by Cooley and collaborators.
687 Cooley et al. (2020) also used the relationships between air temperature and landfast ice
688 break-up date, together with projected changes in air temperature from a set of eight CMIP5
689 global climate models, to project future changes in the breakup dates. Specifically, we note
690 that the trends projected for the remainder of the century in Cooley et al. (2020) are in many
691 instances less pronounced (in days/decade shift in breakup) than those identified here. For
692 example, for Clyde River Cooley et al. project a shift in breakup to an earlier date by 23 days
693 by the year 2099 as compared to changes of a similar magnitude but over a much shorter time
694 period examined here (Fig. 8 and 9). For Clyde River, the comparison between trends in the
695 local break-up timing compared to that for the broader region (Baffin Bay) also reveals that

696 the regional trends are much less pronounced than those at the local scale (Fig. 8 and 9).
697 Furthermore, the two westernmost communities examined by Cooley et al. (2020),
698 Tuktoyaktuk and Paulatuk (Eastern Beaufort Sea), were projected to see earlier landfast ice
699 break-up onset of 5 days and 11 days, respectively, by 2099. The data compiled here for
700 Prudhoe Bay and the Beaufort Sea indicate a substantially larger shift towards earlier dates by
701 more than 5 days *per decade* (Fig. 8 and 9).

702 One other study that addressed future changes of sea ice duration in the Pacific sector of the
703 Arctic is Wang et al.'s (2018) evaluation mid-21st-century projections based on sea ice
704 concentrations simulated by seven CMIP5 global climate models. However, Wang et al.'s
705 evaluations were for the broader offshore areas of the East Siberian, Chukchi and Beaufort
706 Seas rather than for immediate coastal areas, as global climate models generally do not
707 include landfast ice. Pan-Arctic models that simulated landfast ice parameterized
708 thermodynamically without addressing its mobility had significant problems in forecasting
709 coastal ice thickness, especially during freeze-up in September and October (Johnson et al.,
710 2012). The projected increases in ice-free season length over the 2015-2044 period were
711 found were found to vary from about 20 days in the Bering Strait region to up to 60 days in
712 the offshore areas of the East Siberian, Chukchi and Beaufort Seas. While these changes are
713 for offshore areas, they are larger than those projected for coastal areas by late century in the
714 study of Cooley et al. (2020).

715 **5. Conclusion**

716 The primary objective of this study was to use the locally-based metrics to construct
717 indicators of break-up and freeze-up at near-coastal locations in which sea ice has high

718 stakeholder relevance. A set of ten coastal locations distributed around the Arctic were
719 selected for this purpose. The sea ice indicators used here are based on local ice climatologies
720 informed by community ice use (Johnson and Eicken, 2016; Eicken et al., 2014) rather than
721 prescribed “universal” thresholds of ice concentration (e.g., 15%, 80%) used in other recent
722 studies of sea ice break-up and freeze-up.

723 The trends and interannual variations of the local indicators of break-up and freeze-up at the
724 ten nearshore are similar to the trends and variations of corresponding indicators for broader
725 offshore regions, but the site-specific indicators often differ from the regional indicators by
726 several days to several weeks. Relative to indicators for broader adjacent seas, the coastal
727 indicators show later break-up at sites known to have extensive landfast ice, whose break-up
728 typically lags retreat of the adjacent, thinner drifting ice. The coastal indicators also show an
729 earlier freeze-up at some sites in comparison with freeze-up for broader offshore regions,
730 likely tied to earlier freezing of shallow water regions and areas affected by freshwater input
731 from nearby streams and rivers. However, the trends towards earlier break-up and later freeze-
732 up are unmistakable over the post-1979 period at nearly all the coastal sites and their
733 corresponding regional seas.

734 The differences between the coastal and offshore regional indicators matter greatly to local
735 users whose harvesting of coastal resources and Indigenous culture are closely tied to the
736 timing of key events in the seasonal ice cycle (Huntington et al., 2021; Eicken et al., 2014).
737 These differences also matter from the perspective of maritime activities, where access to
738 coastal locations for destination traffic is a key factor (Brigham, 2017). These offsets vary
739 considerably by region. In light of these findings, we view locally as well as regionally
740 defined measures of sea-ice break-up and freeze-up as a key set of indicators linking pan-

741 Arctic or global indicators such as sea-ice extent or volume to local and regional uses of sea
742 ice, with the potential to inform community-scale adaptation and response.

743

744 **Acknowledgments**

745 This work was supported by the Climate Program Office of the National Oceanic and
746 Atmospheric Administration through Grant NA17OAR431060 Additional funding was
747 provided by the Interdisciplinary Research for Arctic Coastal Environments (InterFACE)
748 project through the U.S. Department of Energy, Office of Science, Biological and
749 Environmental Research RGMA program.

750

751 **Data Availability**

752 The daily grids of passive-microwave-derived sea ice concentrations are available from the
753 National Snow and Ice Data Center as dataset NSIDC-0051, available at
754 <https://nsidc.org/data/nsidc-0051>. Lists of the indicator dates for the coastal sites and the
755 MASIE regions are available from the author on request.

756

757 **Author contributions**

758 JEW served the principal investigator for the study, led the drafting of the manuscript, and
759 performed the factor analysis described in Section 3. HE supervised the implementation of
760 the revised indicators for the coastal sites and the MASIE regions, and drafted parts of the
761 text. KR performed the indicator calculations, produced Figures 1-11, and assisted in the

762 preparation of the manuscript. MJ designed the original indicators, participated in the
763 modification of the indicators, and contributed to the revision of the manuscript.

764

765 **Competing interests**

766 The authors declare that they have no conflict of interest

767

768

769 **References**

770 AMAP: Adaptation Actions for a Changing Arctic: Perspectives from the Baffin Bay/Davis
771 Strait Region. Arctic Monitoring and Assessment Programme (AMAP), Oslo, Norway. xvi +
772 354 pp, <https://www.amap.no/documents/download/3015/inline>, 2018.

773 AMAP: Snow, water, ice and permafrost in the Arctic (SWIPA) 2017, Arctic Monitoring and
774 Assessment Programme (AMAP), Oslo, Norway, xiv + 269 pp. 2017.

775

776 Bliss, A.C., and Anderson, M.R.: Arctic sea ice melt onset and timing from passive
777 microwave- and surface air temperature-based methods, *J. Geophys. Res.*, 123, 9063-9080,
778 <https://doi.org/10.1029/2018JD028676>, 2018.

779

780 Bliss, A.C., Steele, M., Peng, G., Meier, W.M., and Dickinson, S: Regional variability of
781 Arctic sea ice seasonal climate change indicators from a passive microwave climate data
782 record, *Environ. Res. Lett.*, 14, 045003, <https://doi.org/10.1088/1748-9326/aafb84>, 2019.

783

784 Box, J.E., and 19 coauthors: Key indicators of Arctic climate change: 1971–2017, *Environ..*
785 *Res. Lett.*, 14(4),.045010, <https://doi.org/10.1088/1748-9326/aafc1b>, 2019.

786

787 Brigham, L.W.: The changing maritime Arctic and new marine operations. In: Beckman, R.
788 C., Henriksen, T., Dalaker Kraabel, K., Molenaar, E. J., and Roach, J. A. (eds.): *Governance*
789 *of Arctic shipping* (pp. 1-23), Brill Nijhoff, 2017.

790

791 Cavalieri, D.J., Gloersen, P., and Campbell, W.J.: Determination of sea ice parameters with
792 the NIMBUS-7 SMMR, *J. Geophys. Res.*, 89(D4): 5355-5369,
793 <https://doi.org/10.1029/JD089iD04p05355>, 1984.

794

795 Cooley, S.W., Ryan, J.C., Smith, L.C., Horvat, C., Pearson, B., Dale, B. and Lynch, A.H.:
796 Coldest Canadian Arctic communities face greatest reductions in shorefast sea ice. *Nature*
797 *Climate Change*, 10(6), pp.533-538.

798 <https://www.nature.com/articles/s41558-020-0757-5>, 2020.

799

800 Comiso, J. C: Characteristics of Arctic Winter Sea Ice from Satellite Multispectral
801 Microwave Observations, *J. Geophys. Res.*, 91(C1), 5C0766, 975-994, 1986
802

803 Dammann, D.O., Eicken, H., Mahoney, A.R., Meyer, F.J. and Betcher, S: Assessing sea ice
804 trafficability in a changing Arctic. *Arctic*, 71(1), 59-75, <https://doi.org/10.14430/arctic4701>,
805 2018.
806

807 Deser, C., Walsh, J.E., and Timlin, M.S.: Arctic sea ice variability in the context of recent
808 atmospheric circulation trends, *J. Climate*, 13, 617-633, [https://doi.org/10.1175/1520-
809 0442\(2000\)013<0617:ASIVIT>2.0.CO;2](https://doi.org/10.1175/1520-0442(2000)013<0617:ASIVIT>2.0.CO;2), 2000.

810 Druckenmiller, M.L. et al.: The Arctic. *Bull. Amer. Meteor. Soc.*, 102, S263-S316,
811 <https://doi.org/10.1175/BAMS-D-21-0086.1>, 2021.

812 Eicken, H., Kaufman, M., Krupnik, I., Pulsifer, P., Apangalook, L., Apangalook, P., Weyapuk
813 Jr, W., and Leavitt, J.: A framework and database for community sea ice observations in a
814 changing Arctic: An Alaskan prototype for multiple users, *Polar Geogr.*, 37(1), 5-27,
815 <http://dx.doi.org/10.1080/1088937X.2013.873090>, 2014.
816

817 Fang, A., and Wallace, J. M.: Arctic sea ice variability on a timescale of weeks in relation to
818 atmospheric forcing, *J. Climate*, 7, 1897-1914, [https://doi.org/10.1175/1520-
819 0442\(1994\)007<1897:ASIVOA>2.0.CO;2](https://doi.org/10.1175/1520-0442(1994)007<1897:ASIVOA>2.0.CO;2), 1994. .
820

821 Fu, D., Liu, B., Yu, G., Huang, H., and Qu, L: Multiscale variations in Arctic sea ice motion
822 and links to atmospheric and oceanic conditions, *The Cryosphere*, 15, 3797-3811,
823 <https://doi.org/10.5194/tc-15-3797-2021>, 2021.
824

825 Hosekova, L., Eidam, E., Panteleev, G., Rainville, L., Rogers, W.E., and Thomson, J.:
826 Landfast ice and coastal wave exposure in northern Alaska. *Geophys. Res. Lett.*, 48(22),
827 e2021GL095103, <https://doi.org/10.1029/2021GL095103>, 2021.
828

829 Huntington, H. P., Raymond-Yakoubian, J., Noongwook, G., Naylor, N., Harris, C.,
830 Harcharek, Q. and Adams, B.: “We never get stuck”: A collaborative analysis of change and
831 coastal community subsistence practices in the northern Bering and Chukchi Seas,
832 *Alaska, Arctic*, 74(2), 113-126, 2021.
833

834 IPCC: Climate Change 2021: The Physical Science Basis. Contribution of Working Group I
835 to the Sixth Assessment Report of the Intergovernmental Panel on Climate Change [Masson-
836 Delmotte, V., Zhai, P., Pirani, A., Connors, S. L., Péan, C., Berger, S., Caud, N., Chen, Y.,
837 Goldfarb, L., Gomis, M. I., Huang, M., Leitzell, K. Lonnoy, E., Matthews, J. B. R., Maycock,
838 T. K., Waterfield, Y., Yelekçi, O., Yu, R., and Zho, B. (eds.)]. Intergovernmental Panel on
839 Climate Change, Cambridge University Press.
840 [https://www.bing.com/search?FORM=AFSCVO&PC=AFSC&q=IPCC+AR6+Working+Gro
841 up+1+report](https://www.bing.com/search?FORM=AFSCVO&PC=AFSC&q=IPCC+AR6+Working+Group+1+report), 2022.
842

843 Johnson, M., and Eicken, H.: Estimating Arctic sea-ice freeze-up and break-up from the
844 satellite record: A comparison of different approaches in the Chukchi and Beaufort Seas,

845 Elementa: Science of the Anthropocene, 4, 000124, doi:10.12952/journal.elementa.000124,
846 2016.

847

848 Johnson, M., et al.: Evaluation of Arctic sea ice thickness simulated by Arctic Ocean Model
849 Intercomparison Project models, *J. Geophys. Res.*, 117, C00D13, doi:10.1029/2011JC007257,
850 2012

851

852 Kapsch, M.L., Eicken, H., and Robards, M.: Sea ice distribution and ice use by indigenous
853 walrus hunters on St. Lawrence Island, Alaska. In *SIKU: Knowing Our Ice* (Krupnik, I.,
854 Aporta, C., Gearheard, S., Laidler, G. J., and Lielsen Holm, L., Eds.), 115-144, Springer,
855 Dordrecht, 2010.

856

857 Krupnik, I., Apangalook, L., and Apangalook, P: “It’s cold, but not cold enough”: Observing
858 ice and climate change in Gambell, Alaska, in *IPY 2007-2008 and beyond*. In *SIKU:*
859 *Knowing Our Ice* (Krupnik, I., Aporta, C., Gearheard, S., Laidler, G. J., and Lielsen Holm, L.,
860 Eds.), 81-114, Springer, Dordrecht, 2010.

861

862 Mahoney, A.R., Eicken H., Gaylord A.G., and Gens R.: Landfast sea ice extent in the
863 Chukchi and Beaufort Seas: The annual cycle and decadal variability. *Cold Reg. Sci.*
864 *Technol.*, 103, 41–56. doi: 10.1016/j.coldregions.2014.03.0033, 2014..

865

866 Mahoney, A.R., Eicken, H., Gaylord, A.G., and Shapiro , L: Alaska landfast sea ice: Links
867 with bathymetry and atmospheric circulation, *J. Geophys. Res.*, 112, C02001,
868 doi:10.1029/2006JC003559, 2007.

869

870 Markus, T., Stroeve J. C., and Miller, J: Recent changes in Arctic sea ice melt onset, freezeup
871 and melt season length, *J. Geophys. Res. (Oceans)*, 114, 1-14,
872 <https://doi.org/10.1029/2009JC005436>, 2009.

873

874 Meier, W., Fetterer, F., Savoie, M., Mallory, S. Duerr, R., and Stroeve, J.: NOAA/NSIDC
875 Climate Data Record of Passive Microwave Sea Ice Concentration, Version 3 (Boulder,
876 Colorado USA; National Snow and Ice Data Center), <https://doi.org/10.7265/N59P2ZTG>,
877 [Accessed 16 January 2022, 2017].

878

879 Noongwook, G.: Native Village of Savoonga, Native Village of Gambell. In Huntington,
880 H.F., and George, J.C.: Traditional knowledge of the bowhead whale (*Balaena mysticetus*)
881 around St. Lawrence Island Alaska, 47-54, 2007.

882

883 Onarheim, I.H., Eldevik, T., Smedsrud, L.H., and Stroeve, J.C.: Seasonal and regional
884 manifestations of Arctic sea ice loss, *J. Climate*, 31, 4917-4932, [https://doi.org/10.1175/JCLI-](https://doi.org/10.1175/JCLI-D-17-0427.1)
885 [D-17-0427.1](https://doi.org/10.1175/JCLI-D-17-0427.1), 2018.

886

887 Peng, G., Steele, M., Bliss, A. C., Meier, W. N., and Dickinson, S: Temporal means and
888 variability of Arctic sea ice melt and freeze season climate indicators using a satellite climate
889 data record, *Remote Sensing*, 10, 1328, <https://doi.org/10.3390/rs10091328>, 2018.

890

891 Petrich, C., Eicken, H., Zhang, J., Krieger, J., Fukamachi, Y., and Ohshima, K.J.: Coastal
892 landfast sea ice decay and breakup in northern Alaska: Key processes and seasonal prediction,
893 J. Geophys. Res., 117, C02003, doi:10.1029/2011JC007339, 2012.
894

895 Selyuzhenok, V., Krumpfen, T., Mahoney, A., Janout, M., and Gerdes, R.: Seasonal and
896 interannual variability of fast ice extent in the southeastern Laptev Sea between 1999 and
897 2013, J. Geophys. Res. Oceans, 120, 7791–7806, doi:10.1002/2015JC011135, 2015.
898

899 Smith, A., and Jahn, A.: Definition differences and internal variability affect the simulated
900 Arctic sea ice melt season, The Cryosphere, 12, 1–20, <https://doi.org/10.5194/tc-13-1-2019>,
901 2019.
902

903 Serreze, M.C., Crawford, A.D., Stroeve, J.C., Barrett, A.P. and Woodgate, R.A.: Variability,
904 trends, and predictability of seasonal sea ice retreat and advance in the Chukchi Sea. J.
905 Geophys. Res. (Oceans), 127, 7308–7325, 2016.
906

907 Stammerjohn, S., Massom, R., Rind, D. and Martinson, D.: Regions of rapid sea ice change:
908 an inter-hemispheric seasonal comparison. Geophys. Res. Lett. 39, L06501, 2017.
909

910 Stroeve, J.C., Crawford, A.D. and Stammerjohn, S.: Using timing of ice retreat to predict
911 timing of fall freeze-up in the Arctic. Geophys. Res. Lett. 43, 6332–6340, 2016.
912

913 Stroeve, J.C., Markus, T., Boisvert, L., Miller, J., and Barrett, A.: Changes in Arctic melt
914 season and implications for sea ice loss. Geophys. Res. Lett., 41, 1216–1225,
915 <https://doi.org/10.1002/2013GL058951>, 2014.
916

917 Stroeve, J., and Notz, D.: Changing state of Arctic sea ice across all seasons. Env. Res. Lett.,
918 13, 102001, <https://doi.org/10.1088/1748-9326/aade56>, 2018.
919

920 Thomson, J., Smith, M., Drushka, K. and Lee, C.: Air-ice-ocean interactions and the delay of
921 autumn freeze-up in the western Arctic Ocean. *Oceanography*,
922 <https://doi.org/10.5670/oceanog.22.124>, 2022.
923

924 USGCRP: Climate Science Special Report: Fourth National Climate Assessment, Volume I
925 (Wuebbles, D.J., Fahey, D.W., Hibbard, K.A., Dokken, D.J., Stewart, B.C., and Maycock,
926 T.K.[eds.]). U.S. Global Change Research Program, Washington, DC, USA, 470 pp., doi:
927 10.7930/J0J964J6, 2017.
928

929 Wang, M., Yang, Q., Overland, J.E., and Stabenro, P.: Sea-ice cover timing in the Pacific
930 Arctic: The present and projections to mid-century by selected CMIP5 models. *Deep Sea*
931 *Research Part II: Topical Studies in Oceanography*, 152, 22–34,
932 <https://www.sciencedirect.com/science/article/pii/S0967064516302132>, 2018
933

934 Walsh, J. E., and Johnson, C. M.: Interannual atmospheric variability and associated
935 fluctuations in Arctic sea ice extent, J. Geophys. Res., 84, 6915–6928,
936 <https://doi.org/10.1029/JC084iC11p06915>, 1979.

937 Yu, Y, Stern, H., Fowler, C., Fetterer, F., and Maslanik. J.: Interannual variability of Arctic
938 landfast ice between 1976 and 2007. *J. Climate*, Vol. 27, 227-243, doi: [10.1175/JCLI-D-13-](https://doi.org/10.1175/JCLI-D-13-00178.1)
939 [00178.1](https://doi.org/10.1175/JCLI-D-13-00178.1), 2014.

940

941

Supplementary material

942
 943
 944
 945
 946
 947
 948
 949
 950
 951
 952
 953
 954
 955
 956
 957
 958
 959
 960
 961
 962
 963
 964
 965
 966
 967
 968
 969
 970
 971

Table S1. Dates (Julian day numbers) corresponding to the modal values (peaks) of the distributions in Figure 4. (Insufficient number of years met Bliss criteria in Central Arctic).

	Break-up Start		Break-up end		Freeze-up start		Freeze-up end	
	J&E	Bliss	J&E	Bliss	J&E	Bliss	J&R	Bliss
Beaufort Sea	145	187	167	208	292	287	296	279
Chukchi Sea	147	177	181	202	315	312	325	302
E. Siberian Sea	150	182	195	207	281	293	280	294
Laptev Sea	140	192	188	207	280	271	285	279
Kara Sea	145	193	190	209	304	299	307	296
Barents Sea	146	164	152	186	315	297	328	302
Greenland Sea	150	177	162	207	308	290	342	280
Baffin Bay	121	152	149	186	331	311	346	324
Canadian Arctic	147	208	190	207	279	274	298	275
Hudson Bay	139	159	177	198	322	317	326	325
Central Arctic	199		200		306		310	
Bering Sea	110	123	123	142	343	337	362	349

972 Table S2. Slopes (least-squares linear regression lines) of the MASIE regions in Figures 5-6
 973 and 8-11. Also shown are the explained variances (r^2 values of the trend lines and their levels
 974 of statistical significance.

975

Region	Indicator Group	Indicator	Slope (days yr ⁻¹)	r ²	significance level
Baffin Bay	Bliss	Day of Advance	0.4	0.57	< 0.01**
Baffin Bay	Bliss	Day of Closing	0.4	0.52	< 0.01**
Baffin Bay	Bliss	Day of Opening	-0.5	-0.74	< 0.01**
Baffin Bay	Bliss	Day of Retreat	-0.7	-0.77	< 0.01**
Baffin Bay	J&E	Break-up End	-0.2	-0.44	< 0.01**
Baffin Bay	J&E	Break-up Start	-0.1	-0.07	0.67
Baffin Bay	J&E	Freeze-up End	0.4	0.57	< 0.01**
Baffin Bay	J&E	Freeze-up Start	0.5	0.71	< 0.01**
Barents Sea	Bliss	Day of Advance	1.3	0.7	< 0.01**
Barents Sea	Bliss	Day of Closing	1.3	0.7	< 0.01**
Barents Sea	Bliss	Day of Opening	-1.1	-0.72	< 0.01**
Barents Sea	Bliss	Day of Retreat	-1.2	-0.79	< 0.01**
Barents Sea	J&E	Break-up End	-1.0	-0.72	< 0.01**
Barents Sea	J&E	Break-up Start	-0.4	-0.38	0.02*
Barents Sea	J&E	Freeze-up End	1.0	0.72	< 0.01**
Barents Sea	J&E	Freeze-up Start	1.0	0.8	< 0.01**
Beaufort Sea	Bliss	Day of Advance	0.8	0.61	< 0.01**
Beaufort Sea	Bliss	Day of Closing	0.9	0.63	< 0.01**
Beaufort Sea	Bliss	Day of Opening	-0.7	-0.51	< 0.01**
Beaufort Sea	Bliss	Day of Retreat	-1.0	-0.56	< 0.01**
Beaufort Sea	J&E	Break-up End	-0.7	-0.48	< 0.01**
Beaufort Sea	J&E	Break-up Start	-0.6	-0.51	< 0.01**

Beaufort Sea	J&E	Freeze-up End	0.7	0.68	< 0.01**
Beaufort Sea	J&E	Freeze-up Start	0.7	0.65	< 0.01**
Bering Sea	Bliss	Day of Advance	0.4	0.43	< 0.01**
Bering Sea	Bliss	Day of Closing	0.4	0.36	0.02*
Bering Sea	Bliss	Day of Opening	-0.2	-0.28	0.09
Bering Sea	Bliss	Day of Retreat	-0.3	-0.37	0.02*
Bering Sea	J&E	Break-up End	-0.0	-0.01	0.98
Bering Sea	J&E	Break-up Start	0.0	0.05	0.77
Bering Sea	J&E	Freeze-up End	0.3	0.33	0.04*
Bering Sea	J&E	Freeze-up Start	0.5	0.65	< 0.01**
Canadian Arch.	Bliss	Day of Advance	0.5	0.63	< 0.01**
Canadian Arch.	Bliss	Day of Closing	0.6	0.56	< 0.01**
Canadian Arch.	Bliss	Day of Opening	-0.3	-0.57	< 0.01**
Canadian Arch.	Bliss	Day of Retreat	-0.9	-0.7	< 0.01**
Canadian Arch.	J&E	Break-up End	-0.4	-0.62	< 0.01**
Canadian Arch.	J&E	Break-up Start	-0.4	-0.5	< 0.01**
Canadian Arch.	J&E	Freeze-up End	0.3	0.58	< 0.01**
Canadian Arch.	J&E	Freeze-up Start	0.2	0.51	< 0.01**
Central Arctic	Bliss	Day of Closing	0.7	0.33	0.04*
Central Arctic	Bliss	Day of Opening	-0.5	-0.17	0.31
Central Arctic	J&E	Break-up End	-1.0	-0.36	0.03*
Central Arctic	J&E	Break-up Start	-0.9	-0.31	0.06
Central Arctic	J&E	Freeze-up End	0.1	0.03	0.88
Central Arctic	J&E	Freeze-up Start	0.6	0.18	0.31
Chukchi Sea	Bliss	Day of Advance	1.0	0.75	< 0.01**
Chukchi Sea	Bliss	Day of Closing	1.1	0.73	< 0.01**

Chukchi Sea	Bliss	Day of Opening	-0.7	-0.71	< 0.01**
Chukchi Sea	Bliss	Day of Retreat	-0.7	-0.66	< 0.01**
Chukchi Sea	J&E	Break-up End	-0.6	-0.65	< 0.01**
Chukchi Sea	J&E	Break-up Start	-0.5	-0.46	< 0.01**
Chukchi Sea	J&E	Freeze-up End	0.8	0.69	< 0.01**
Chukchi Sea	J&E	Freeze-up Start	1.0	0.79	< 0.01**
E. Siberian Sea	Bliss	Day of Advance	0.8	0.74	< 0.01**
E. Siberian Sea	Bliss	Day of Closing	1.1	0.78	< 0.01**
E. Siberian Sea	Bliss	Day of Opening	-0.7	-0.51	< 0.01**
E. Siberian Sea	Bliss	Day of Retreat	-0.8	-0.6	< 0.01**
E. Siberian Sea	J&E	Break-up End	-0.5	-0.45	< 0.01**
E. Siberian Sea	J&E	Break-up Start	-0.7	-0.46	< 0.01**
E. Siberian Sea	J&E	Freeze-up End	0.6	0.76	< 0.01**
E. Siberian Sea	J&E	Freeze-up Start	0.7	0.77	< 0.01**
Greenland Sea	Bliss	Day of Advance	0.9	0.62	< 0.01**
Greenland Sea	Bliss	Day of Closing	0.5	0.45	< 0.01**
Greenland Sea	Bliss	Day of Opening	-0.4	-0.38	0.02*
Greenland Sea	Bliss	Day of Retreat	-0.6	-0.5	< 0.01**
Greenland Sea	J&E	Break-up End	-0.3	-0.32	0.05*
Greenland Sea	J&E	Break-up Start	-0.0	-0.04	0.79
Greenland Sea	J&E	Freeze-up End	0.4	0.38	0.02*
Greenland Sea	J&E	Freeze-up Start	0.7	0.63	< 0.01**

Hudson Bay	Bliss	Day of Advance	0.5	0.64	< 0.01**
Hudson Bay	Bliss	Day of Closing	0.4	0.57	< 0.01**
Hudson Bay	Bliss	Day of Opening	-0.5	-0.67	< 0.01**
Hudson Bay	Bliss	Day of Retreat	-0.7	-0.74	< 0.01**
Hudson Bay	J&E	Break-up End	-0.4	-0.65	< 0.01**
Hudson Bay	J&E	Break-up Start	-0.1	-0.06	0.72
Hudson Bay	J&E	Freeze-up End	0.4	0.55	< 0.01**
Hudson Bay	J&E	Freeze-up Start	0.6	0.73	< 0.01**
Kara Sea	Bliss	Day of Advance	0.7	0.63	< 0.01**
Kara Sea	Bliss	Day of Closing	0.9	0.66	< 0.01**
Kara Sea	Bliss	Day of Opening	-1.0	-0.75	< 0.01**
Kara Sea	Bliss	Day of Retreat	-1.1	-0.76	< 0.01**
Kara Sea	J&E	Break-up End	-0.9	-0.7	< 0.01**
Kara Sea	J&E	Break-up Start	-0.3	-0.22	0.18
Kara Sea	J&E	Freeze-up End	0.8	0.62	< 0.01**
Kara Sea	J&E	Freeze-up Start	0.7	0.64	< 0.01**
Laptev Sea	Bliss	Day of Advance	0.6	0.65	< 0.01**
Laptev Sea	Bliss	Day of Closing	0.7	0.64	< 0.01**
Laptev Sea	Bliss	Day of Opening	-0.6	-0.55	< 0.01**
Laptev Sea	Bliss	Day of Retreat	-0.7	-0.58	< 0.01**
Laptev Sea	J&E	Break-up End	-0.6	-0.52	< 0.01**
Laptev Sea	J&E	Break-up Start	-0.7	-0.48	< 0.01**
Laptev Sea	J&E	Freeze-up End	0.4	0.68	< 0.01**
Laptev Sea	J&E	Freeze-up Start	0.4	0.64	< 0.01**

976

977

978 Table S3. Same as Table S2, but for the local indicators. Slopes (linear regression lines)
 979 correspond to Figures 8-11. Also shown are the explained variances (r^2 values of the trend
 980 lines and their levels of statistical significance.

981

Location	Indicator Group	Indicator	Slope (days yr ⁻¹)	r ²	Significance level
Churchill	Bliss	Day of Advance	0.3	0.52	< 0.01**
Churchill	Bliss	Day of Closing	0.4	0.51	< 0.01**
Churchill	Bliss	Day of Opening	-0.8	-0.59	< 0.01**
Churchill	Bliss	Day of Retreat	-1.0	-0.67	< 0.01**
Churchill	J&E	Break-up End	-0.7	-0.54	< 0.01**
Churchill	J&E	Break-up Start	-0.5	-0.3	0.07
Churchill	J&E	Freeze-up End	0.4	0.49	< 0.01**
Churchill	J&E	Freeze-up Start	0.7	0.53	< 0.01**
Clyde River	Bliss	Day of Advance	0.3	0.46	< 0.01**
Clyde River	Bliss	Day of Closing	0.3	0.45	< 0.01**
Clyde River	Bliss	Day of Opening	-0.6	-0.47	< 0.01**
Clyde River	Bliss	Day of Retreat	-0.5	-0.42	< 0.01**
Clyde River	J&E	Break-up End	-0.6	-0.5	< 0.01**
Clyde River	J&E	Break-up Start	-0.5	-0.22	0.18
Clyde River	J&E	Freeze-up End	0.3	0.45	< 0.01**
Clyde River	J&E	Freeze-up Start	0.3	0.43	< 0.01**
Mestersvig	Bliss	Day of Advance	0.6	0.36	0.05*
Mestersvig	Bliss	Day of Closing	0.9	0.52	< 0.01**
Mestersvig	Bliss	Day of Opening	-0.7	-0.36	0.02*
Mestersvig	Bliss	Day of Retreat	-0.6	-0.37	0.04*
Mestersvig	J&E	Break-up End	-0.2	-0.2	0.26
Mestersvig	J&E	Break-up Start	0.1	0.04	0.83

Mestersvig	J&E	Freeze-up End	0.6	0.5	< 0.01**
Mestersvig	J&E	Freeze-up Start	0.5	0.42	0.02*
Pevek	Bliss	Day of Advance	1.1	0.72	< 0.01**
Pevek	Bliss	Day of Closing	1.1	0.77	< 0.01**
Pevek	Bliss	Day of Opening	-0.9	-0.4	0.01*
Pevek	Bliss	Day of Retreat	-1.0	-0.46	< 0.01**
Pevek	J&E	Break-up End	-0.7	-0.33	0.05
Pevek	J&E	Break-up Start	-1.1	-0.37	0.03*
Pevek	J&E	Freeze-up End	0.8	0.76	< 0.01**
Pevek	J&E	Freeze-up Start	0.9	0.73	< 0.01**
Prudhoe Bay	Bliss	Day of Advance	0.8	0.52	< 0.01**
Prudhoe Bay	Bliss	Day of Closing	0.8	0.65	< 0.01**
Prudhoe Bay	Bliss	Day of Opening	-1.0	-0.56	< 0.01**
Prudhoe Bay	Bliss	Day of Retreat	-0.9	-0.51	< 0.01**
Prudhoe Bay	J&E	Break-up End	-0.8	-0.54	< 0.01**
Prudhoe Bay	J&E	Break-up Start	-0.5	-0.27	0.1
Prudhoe Bay	J&E	Freeze-up End	0.8	0.6	< 0.01**
Prudhoe Bay	J&E	Freeze-up Start	0.7	0.59	< 0.01**
Sabetta	Bliss	Day of Advance	0.4	0.55	< 0.01**
Sabetta	Bliss	Day of Closing	0.4	0.47	< 0.01**
Sabetta	Bliss	Day of Opening	-0.9	-0.59	< 0.01**
Sabetta	Bliss	Day of Retreat	-1.0	-0.78	< 0.01**
Sabetta	J&E	Break-up End	-0.8	-0.56	< 0.01**
Sabetta	J&E	Break-up Start	-0.9	-0.42	< 0.01**
Sabetta	J&E	Freeze-up End	0.4	0.41	< 0.01**
Sabetta	J&E	Freeze-up Start	0.4	0.56	< 0.01**

South Chukchi Sea	Bliss	Day of Advance	0.9	0.63	< 0.01**
South Chukchi Sea	Bliss	Day of Closing	0.7	0.58	< 0.01**
South Chukchi Sea	Bliss	Day of Opening	-0.6	-0.51	< 0.01**
South Chukchi Sea	Bliss	Day of Retreat	-0.7	-0.56	< 0.01**
South Chukchi Sea	J&E	Break-up End	-0.6	-0.52	< 0.01**
South Chukchi Sea	J&E	Break-up Start	-0.6	-0.39	0.02*
South Chukchi Sea	J&E	Freeze-up End	0.7	0.57	< 0.01**
South Chukchi Sea	J&E	Freeze-up Start	0.8	0.63	< 0.01**
St. Lawrence Island	Bliss	Day of Advance	0.6	0.33	0.05*
St. Lawrence Island	Bliss	Day of Closing	0.3	0.2	0.24
St. Lawrence Island	Bliss	Day of Opening	-0.1	-0.16	0.35
St. Lawrence Island	Bliss	Day of Retreat	-0.3	-0.28	0.09
St. Lawrence Island	J&E	Break-up End	-0.1	-0.11	0.49
St. Lawrence Island	J&E	Break-up Start	-0.0	-0.02	0.92
St. Lawrence Island	J&E	Freeze-up End	0.4	0.25	0.13
St. Lawrence Island	J&E	Freeze-up Start	0.5	0.33	0.04*
Tiksi	Bliss	Day of Advance	0.2	0.36	0.02*
Tiksi	Bliss	Day of Closing	0.2	0.41	0.01*

Tiksi	Bliss	Day of Opening	-0.4	-0.54	< 0.01**
Tiksi	Bliss	Day of Retreat	-0.6	-0.54	< 0.01**
Tiksi	J&E	Break-up End	-0.3	-0.53	< 0.01**
Tiksi	J&E	Break-up Start	-0.3	-0.34	0.03*
Tiksi	J&E	Freeze-up End	0.3	0.45	< 0.01**
Tiksi	J&E	Freeze-up Start	0.2	0.45	< 0.01**
Utqiaf°vik	Bliss	Day of Advance	1.1	0.6	< 0.01**
Utqiaf°vik	Bliss	Day of Closing	1.1	0.67	< 0.01**
Utqiaf°vik	Bliss	Day of Opening	-1.2	-0.52	< 0.01**
Utqiaf°vik	Bliss	Day of Retreat	-1.2	-0.71	< 0.01**
Utqiaf°vik	J&E	Break-up End	-0.7	-0.52	< 0.01**
Utqiaf°vik	J&E	Break-up Start	-0.7	-0.27	0.11
Utqiaf°vik	J&E	Freeze-up End	0.8	0.66	< 0.01**
Utqiaf°vik	J&E	Freeze-up Start	0.9	0.62	< 0.01**

982

983

984

985

986